Evolution of genotypic and phenotypic diversity in multispecies biofilms

Cristina I. Amador[1], Sofia Zoe Moscovitz[1], Lorrie Maccario[1], Jakob Herschend[1 2], Isabel-Sophie Kramer[1], Hannah Jeckel[3], Vaughn S. Cooper[4], Knut Drescher[3], Thomas R. Neu[5], Mette Burmølle[1] and Henriette L. Røder[6 #]

[1]Section of Microbiology, Department of Biology, University of Copenhagen, Copenhagen, Denmark

[2]Present address: Functional Food, Novozymes A/S, 2800, Lyngby, Denmark

[3]Biozentrum, University of Basel, Switzerland

[4]University of Pittsburgh, Pittsburgh, USA

[5]Department of River Ecology, Helmholtz Centre for Environmental Research - UFZ, Magdeburg, Germany

[6]Section for Food Microbiology, Gut Health, and Fermentation. Department of Food Science, University of Copenhagen. Rolighedsvej 26, 1958 Frederiksberg C, Denmark.

Author correspondence to h.lyng.roeder@food.ku.dk

Running title: Evolution in structured and non-structured communities

Keywords: multispecies, bacterial interactions, biofilm, matrix, adaptive evolution, sporulation

Author contributions

CIA is first author. Conceptualization and planning: HLR. Execution of experiments: CIA, HLR. SZM, ISK. Data analysis: CIA, HLR and LM. Manuscript preparation: CIA, HLR and MB, in consultation with JH, HJ, VSC, KD, TRN.

Abstract

Bacterial fitness and adaptability in microbial communities are influenced by interspecies interactions and spatial organization. This study investigated how these factors shape the evolutionary dynamics of *Bacillus thuringiensis*. A distinct phenotypic variant of *B. thuringiensis* emerged consistently under both planktonic and biofilm conditions, as well as in monospecies and mixed-species settings, but was strongly selected in biofilms and during coexistence with *Pseudomonas defluvii* and/ or *Pseudomonas brenneri*. Compared to its ancestor, the variant exhibited shorter generation times, reduced sporulation, auto-aggregation, and lower biomass in mixed-species biofilms. Mutations in the *spo0A* regulator, which controls sporulation and biofilm matrix production, were identified in all variants. Proteomics revealed a reduction in TasA, a key matrix protein, in the variant but increased levels in co-culture with *P. brenneri*. These findings highlight how interspecies interactions drive *B. thuringiensis* diversification, promoting traits like reduced matrix production and species coexistence, with implications for microbial consortia applications in agriculture and biopesticides.

Introduction

When encountering new environmental challenges, bacterial populations can adapt their physiological state (phenotype) through different mechanisms: expressing specific traits, acquiring new advantageous mutations (*de novo* genetic variation), or utilizing the pre-existing genetic diversity within the population (standing genetic variation) [1–3]. Besides intraspecific variation, natural communities contain many species that might either constrain adaptation by competing for resources, e.g., via niche exclusion [4], or facilitate adaptation by making new niches available [5, 6]. In biofilms, microbial cells are in close proximity and can influence each other´s phenotypes and evolutionary trajectories through social interactions [7]. Spatial segregation in biofilms increases the frequency of interactions between cells of the same genotype and favors cooperative behaviors but can also support variants that are otherwise outcompeted in unsegregated environments [8–10] and facilitate coexisting populations [11, 12]. Several studies have reported that competitive interactions within biofilms are dominant, including competition for limited space and resources [10, 13–16]. However, evidence shows that competition can subside locally over time, often leading to stable coexistence [17]. We have previously described that interspecies interactions can lead to evolved variants that display enhanced mutualism in biofilms [18–20]. Thus, to better understand bacterial adaptation mechanisms in natural environments, investigations of adaptation mechanisms in the presence of spatial structure and multiple species that co-occur in natural communities are crucial.

The evolution of social interactions within biofilms has been extensively studied in various Gram-negative bacteria, including *Pseudomonas spp*. and *Burkholderia cenocepacia* [21–23]. However, comparatively less attention has been devoted to investigating evolutionary processes of Gram-positive bacteria, especially in the presence of multiple species. While both bacterial groups may be subjected to similar evolutionary forces, they possess distinct biological and ecological features, which may lead to divergent adaptive dynamics. Although some studies have explored the adaptive evolution of Gram-positive bacteria in diverse biofilm systems, their focus has primarily been on adaptive genotypes [24–26] or co-

60 culture [20, 27]. Such limited focus leaves a gap in our understanding of how Gram-positive bacteria evolve
61 within complex, multispecies biofilms.

62 In this study, we aim to investigate how cultivation conditions—specifically spatial structure
63 (biofilm *vs.* planktonic settings) and interspecies interactions (mono-, dual- or multispecies)— influence
64 the diversification of *Bacillus thuringiensis* (BT), a Gram-positive, spore-forming bacterium renowned for
65 its insecticidal capabilities [28]. BT was cultured in isolation and in combination with *Pseudomonas defluvii*
66 (PD) and *Pseudomonas brenneri* (PB), both of which were co-isolated with BT from a wastewater treatment
67 facility in Kalundborg, Denmark [29]. *Bacillus* spp. and *Pseudomonas* spp. are known for their utility as
68 plant growth enhancers and biopesticides [30]. Importantly, research has demonstrated that such bacterial
69 consortia manifest unique, emergent properties not attainable by individual species alone [31]. Additionally,
70 the rationale behind selecting these species for our investigation stemmed from their potential synergistic
71 contributions to biofilm formation, a premise supported by preliminary laboratory findings. Other studies
72 on laboratory adaptive evolution employed biofilm settings focusing on biofilm dispersal and
73 recolonization over short evolutionary spans [20, 32]. However, our work aimed at investigating the
74 dynamics of cells that remained in the biofilm, attached to plastic slides. This led to the identification of a
75 phenotypic variant of BT, termed "light variant," from its reduced Congo red dye binding in colonies on
76 agar, compared to the ancestral strain. Morphotypic colony diversification often reflects underlying
77 genotypic changes, which play a crucial role in shaping biofilm formation and adaptation [18, 33, 34].
78 Therefore, we isolated and characterized such light variants, which arose frequently. We found that the light
79 variant colony morphotype was linked to mutations in sporulation genes, and that these variants
80 demonstrated a remarkable ability to dominate and replace the wild-type phenotype in most conditions
81 examined. Crucially, the fitness of this evolved phenotype was enhanced in mixed-species cultures and
82 within biofilm contexts, underlining the effects of both biotic and abiotic complexity on evolutionary
83 dynamics. This finding sheds light on the adaptive strategies of BT within microbial consortia.

Results

Emergence of a BT phenotypic variant after short-term evolution assay

We investigated how the presence of other species influenced the selection of new phenotypic variants of BT under biofilm or planktonic conditions. For the biofilm condition, cells were incubated in TSB with a submerged polycarbonate slide. Prior to transferring the slides, we removed and discarded the floating pellicle, when present, since our evolution experiment targeted surface-adhered cells. The polycarbonate slides were then removed from the well and washed with PBS to remove unattached cells, and transferred to new wells containing fresh media, followed by incubation for another 24 h. This process was repeated for eight consecutive cycles. On day 8, we plated and enumerated the cultures based on distinct colony morphology (Figure 1a). Although not all genetic changes manifest in noticeable physical properties, genetic variation can drive morphotypic colony variation, especially in biofilm settings [18, 33, 34]. In this study, we focused on selecting variants of BT forming colonies of varying morphotypes, by employing TSA Congo Red. Congo red binds different biofilm matrix components, including amyloids and polysaccharides [35, 36]. Thus, altered colony morphology on Congo red agar could provide a visual marker of the underlying genetic changes.

A particular BT phenotypic variant was detected in all replicate evolution experiments, which we termed "light variant" as it bound less Congo red compared to the ancestor (Figure 1a). Colonies exhibiting phenotypic traits indistinguishable from those of the ancestral BT strain— derived from the evolution experiment—are referred to as wild-type phenotype throughout this study. When comparing within colony phenotype depending on the culture condition (wild-type mono-culture *vs.* co-culture; or variant mono-culture *vs.* co-culture), no significant differences in population size were detected ($p > 0.05$, Dunn's post-hoc test; Figure 1b and Supplementary Table 1). However, when comparing BT wild-type and light variant colony phenotypes per culture condition, the latter emerged independently in each evolved biofilm population where it consistently grew to significantly higher CFU counts than the wild-type phenotype ($p < 0.05$, Dunn's post-hoc test; Figure 1b and Supplementary Table 1).

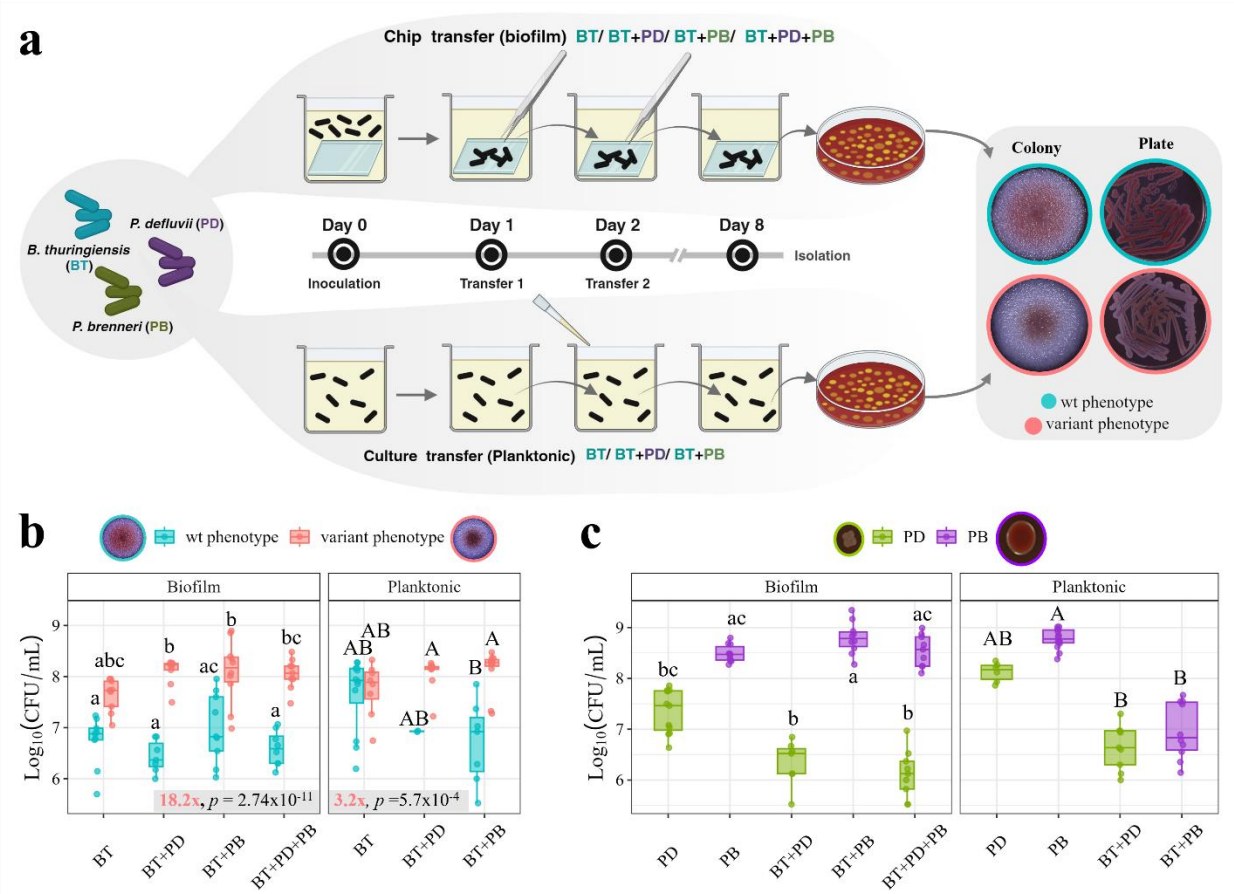

Figure 1. Short-term evolution assay of *Bacillus thuringiensis* (BT) in the presence/absence of *Pseudomonas* species. (a) Experimental setup: BT was cultured alone or with *Pseudomonas brenneri* (PB) and/or *Pseudomonas defluvii* (PD) in Tryptic Soy Broth (TSB) medium, either as planktonic or biofilm cultures, for 24 hours. Biofilm samples were transferred daily onto fresh medium for eight consecutive days, followed by plating on day 8 and CFU counting on TSB agar supplemented with 40 µg/mL Congo red and 20 µg/mL Coomassie brilliant blue (G). **(b)** BT cell counts (Log_{10}(CFU/mL)) of variant (red) and wild-type (blue) phenotypes in different strain combinations after the evolution experiment, presented for biofilm (left) and planktonic (right) cultures. Box plots represent ≥ 3 biological replicates, represented as individual points, each averaged from 3 technical replicates. Different letters denote significance per facet (Dunn´s post-hoc test, $p < 0.05$, Bonferroni correction). Gray boxes represent CFU/mL ratios of variant *vs*. wild-type phenotypes within each setting (biofilm or planktonic) and statistical significance of such ratios (Wilcoxon's test comparing variant and wild-type phenotypes per setting, $p < 0.05$). **(c)** Cell counts (Log_{10}(CFU/mL)) of PD (green) and PB (purple) in various strain combinations and culture conditions after the evolution experiment. Box plots represent ≥ 7 biological replicates, represented as in (b). Different letters denote significance per facet (Dunn´s post-hoc test, $p < 0.05$, Bonferroni correction).

On the contrary, analogous evolution experiments in planktonic culture only showed significant difference in CFU counts between the wild-type and light variant phenotypes in co-culture with PB ($p = 5.07x10^{-04,}$ Dunn's post-hoc test; Figure 1b and Supplementary Table 1). Still, the variant phenotype was

128 found to be significantly more prevalent than the wild-type phenotype regardless of the cultivation
129 settings— biofilm or planktonic— when not considering the species combination (Wilcoxon's test, p_{Biofilm}
130 $= 2.74\text{x}10^{-11}$; $p_{\text{Plank}} = 5.7\text{x}10^{-05}$, Figure 1b). However, the CFU/ mL ratio of variant to wild-type phenotype
131 was substantially higher in biofilm compared to planktonic settings (Ratio variant-wt: biofilm = 18.2-fold;
132 planktonic = 3.2-fold, Figure 1b). To ensure statistical robustness, we re-analyzed the data excluding the
133 BT + PD + PB treatment from the biofilm condition. Nonetheless, the variant still emerged at significantly
134 higher frequency than the wild-type phenotype under biofilm conditions (Ratio variant-wt = 12.2-fold,
135 $p_{\text{Biofilm}} = 2.32\text{x}10^{-08}$, Wilcoxon's test), supporting the conclusion that biofilm evolution enhances variant
136 emergence. Hence, our results from short-term evolution experiments suggest that the BT light variant
137 exhibited higher fitness under biofilm conditions and in the presence of PB and/or PD when compared to
138 the wild-type colony phenotype.

139 During the evolution experiment, all species were maintained. However, the trajectories of the
140 *Pseudomonas* species varied depending on the culture condition and design, as shown in Figure 1c. BT
141 showed a competitive interaction with both *Pseudomonas* species in planktonic settings (Figure 1c, right
142 panel). Specifically, the presence of BT reduced the number of PB cells by 1.92 Log_{10} (Dunn's post-hoc
143 test; $p = 2.7\text{x}10^{-05}$, Log_{10} CFU/mL: BT+PB = 6.88; PB = 8.8). These findings indicate that the lack of spatial
144 structure and resulting intermixing may limit the co-existence of different species. However, this was not
145 observed under biofilm conditions, where no significant differences were observed in *Pseudomonas*
146 populations, despite the presence/ absence of BT ($p = 1.0$, Dunn's post-hoc test; Figure 1c). This suggests
147 that the adapted BT phenotype may facilitate the co-existence of BT and PB in biofilm settings.

148 **The BT "light variant" exhibited distinct phenotypic traits compared to its ancestor**

149 We isolated 150 BT colonies of both light and wild-type phenotype (50% of each) from
150 independent evolution experiments and conditions. All colonies within each phenotype group (light or wild
151 type) displayed similar phenotypic traits. The BT light variant displayed different colony morphology
152 compared to the ancestral BT strain, because of reduced Congo red binding (Figure 1a). Congo red binds

153 to different biofilm matrix components, including amyloids and polysaccharides [35, 36]. Furthermore, the
154 wild-type and light variant phenotypes also had visibly different phenotypes during growth in planktonic
155 cultures: under non-shaking conditions, the ancestral BT cells sank to the bottom of the culture, while cells
156 of the light variant remained in suspension (Figure 2a). Auto-aggregation, where bacteria attach to each
157 other rather than to a surface, is observed in many bacterial species. This behavior involves the formation
158 of macroscopic cell aggregates that settle at the bottom of culture tubes. [37, 38]. Moreover, some
159 environmental *Bacillus licheniformis* have been documented to undergo aggregation during suspension
160 culture under carbon limitation or glucose-free conditions [39, 40].

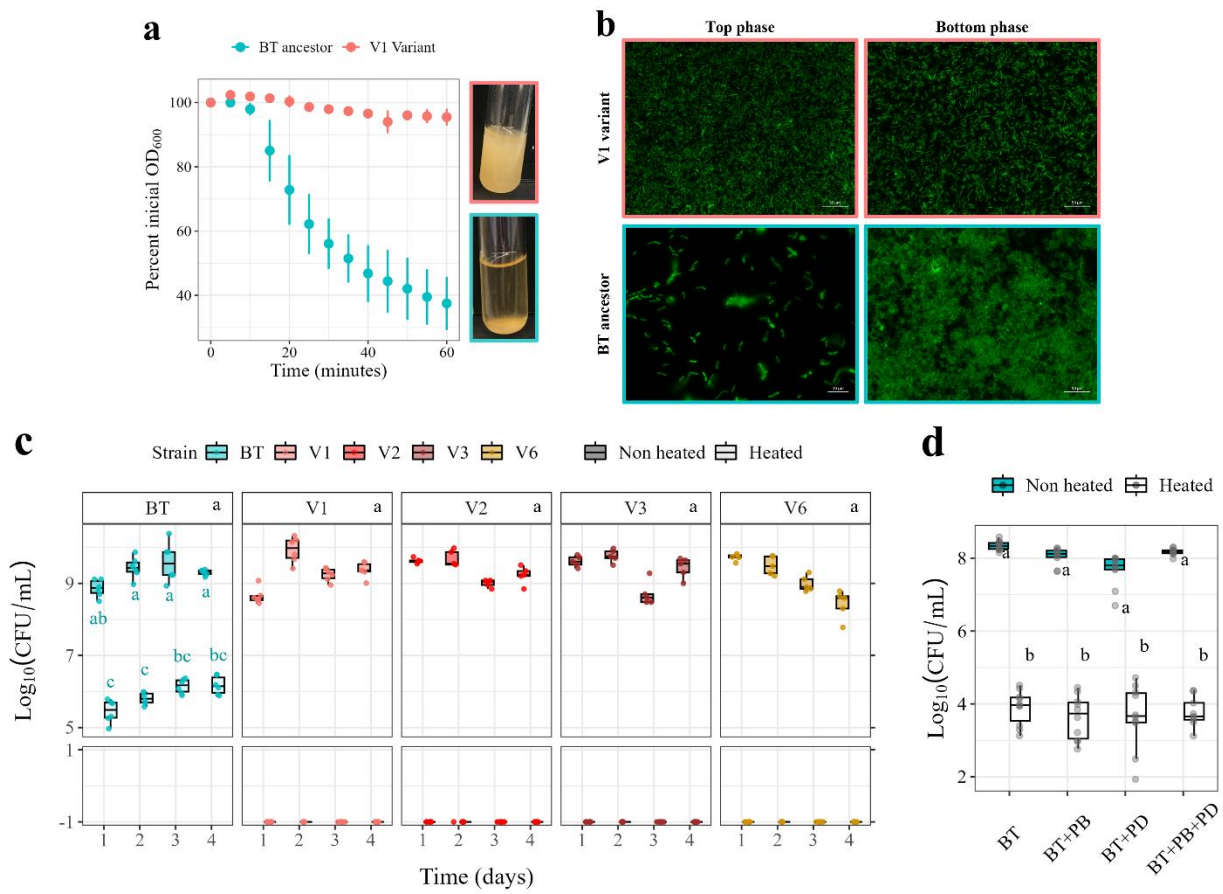

161
162 **Figure 2. Phenotypic features of *B. thuringiensis* ancestor and adapted variant strains. (a)**
163 Sedimentation pattern of BT ancestor and V1 variant strains in TSB planktonic cultures. Sedimentation
164 dynamics was measured as the decay of initial OD_{600} over time, represented as the mean OD_{600} percentage
165 relative to initial OD_{600} (t_0). Data based on 3 biological replicates. In the absence of shaking, sedimentation
166 can be observed only for the ancestor strain. **(b)** Auto-aggregative phenotype of BT ancestral strain
167 compared to the adapted variant. Images show top and bottom phases of planktonic cultures in TSB stained

168 with 10 µM SYTO 16 nucleic acid cell stain. Images were acquired with a Zeiss Axio Observer Z1
169 epifluorescence microscope with a LD-NEOFLUAR 20x objective. Scale bars represent 50 µm. **(c)** Spore
170 formation ability of *B. thuringiensis* ancestral (BT) and variant strains under control (vegetative cells, non-
171 heated) and boiling (germinating spores, heated) conditions in planktonic monocultures over 1-4 days
172 incubation. Log_{10}(CFU/mL) values were adjusted by adding 0.1 to accommodate zero values (represented
173 as -1). n ≥ 5 biological replicates. Different letters denote significant differences ($p < 0.05$, Dunn´s post-
174 hoc test, Bonferroni correction). Black letters denote significant differences between strains only
175 considering non-heated conditions, while turquoise letters indicate comparisons within BT (heated *vs.* non-
176 heated). **(d)** Spore formation ability of BT ancestral strain in biofilm settings in different strain
177 combinations after one-day incubation; n ≥10 biological replicates.

178 We quantified aggregation by measuring the percentage of initial OD_{600} remaining in suspension
179 over time, using the variant and ancestral BT strains. The variant cells remained mainly in suspension
180 (95%), whereas the ancestral BT strain showed higher cell sedimentation, retaining only 37% of its initial
181 OD_{600} (Figure 2a). Additionally, we also investigated aggregation in both strains by microscopic analysis.
182 For this, we stained top and bottom phases of planktonic cultures for both strains with the nucleic acid stain
183 SYTO 16. We found that the ancestral BT strain predominantly formed cell clusters in the bottom phase,
184 whereas the variant consisted mainly of single cells regardless of the visualized phase (Figure 2b). Thus,
185 we confirm that the observed sedimentation by the BT ancestor is linked to auto-aggregation, whereas cells
186 of the variant phenotype do not aggregate to the same extent.

187 In addition to these phenotypic traits, the BT light variant was unable to produce spores unlike the
188 ancestral BT strain, as evidenced by optical microscopy (not shown). Given that all variant phenotype
189 colonies displayed similar phenotypic traits, we focused on four light variants, namely V1, V2, V3, and V6,
190 and further investigated their characteristics. These light variants were selected from different culture
191 conditions and evolutionary lineages (independent evolutionary experiments): V1 and V2 were isolated
192 from biofilm co-cultures with PB in different lineages (B and C, respectively), whereas V3 and V6 were
193 isolated from BT biofilm mono-cultures (lineages B and C, respectively) (Supplementary Table 2).

194 We measured the capacity for spore formation of both ancestral and variant strains in planktonic
195 settings over four days. These assays demonstrated that the variants did not produce spores, whereas the
196 ancestral BT strain consistently produced spores regardless of the incubation time (Figure 2c). Next, we

197 investigated whether other species may influence spore formation in the ancestor. The ability to form spores
198 was assessed in mono-, two-species-, or multispecies biofilm conditions for 24-hour biofilms; however, no
199 significant difference was observed between the tested combinations (Dunn´s post-hoc test, $p > 0.05$; Figure
200 2d).

201 We hypothesized that selection for faster growth may have favored the loss of spore production in
202 BT light variants, as sporulation is an energy-intensive process. Growth curves were performed for the BT
203 ancestral and light variant strain in TSB. We found that the four BT light variants consistently showed a
204 significantly faster doubling time (t_{gen}) and growth rate (r) compared to their ancestor (Supplementary Table
205 3). Consequently, the time required to reach half of the maximum culture yield was significantly lower (t_{mid}
206 or ½ k). This data suggests that the BT light variants have a growth advantage compared to the ancestral
207 BT when competing for resources with the *Pseudomonas* species. This may also have led to the higher CFU
208 counts observed in mixed-species cultures during our short-term evolution experiments in biofilms and
209 planktonic cultures.

210 **BT light variants displayed mutations in sporulation-related genes**

211 Whole genome sequencing of BT light variants and the BT ancestor revealed that the light variants
212 displayed mutations in sporulation-related genes. This correlated with the observed lack of sporulation in
213 all variants. Variants V1, V3, and V6 contained distinct mutations resulting in loss of function of the *spo0A*
214 gene, as shown in Supplementary Figure 1a). The *spo0A* gene encodes a response regulator that, in its
215 phosphorylated active form, activates the transcription of early sporulation genes and, consequently, the
216 initiation of sporulation (Supplementary Figure 1b) [41, 42]. For variants V1 and V3, large deletions were
217 observed in this region. Specifically, V1 lacked a 1.5 kb fragment containing most of *spo0A* and CDS0080
218 genes, whereas V3 had a 4.5 kb deletion that also included the *spoIVB* and *recN* genes (Supplementary
219 Figure 1a). V6 only contained a non-synonymous mutation in the *spo0A* gene (C151>T), resulting in a
220 change in the amino acid sequence Q51>stop, leading to early termination and, thus, loss of function of
221 Spo0A. These mutations, confirmed by Sanger sequencing using specific primers (data not shown),

222 undoubtedly explain the non-sporulating phenotype for variants V1, V3, and V6, given the central role of
223 *spo0A* and *spoIVB* in the sporulation process. In regards to variant V2, we didn´t find mutations in *spo0A*
224 but structural variation in the *soj* gene, that is, large-scale changes in the structure of DNA [43]. Soj exerts
225 a dual role in chromosome partitioning and sporulation, particularly in regulating chromosome dynamics
226 as the cell undergoes significant structural changes [44]. All the mutations found in the variants are listed
227 in Supplementary Table 4.

228 Additionally, variant V1 lacked 83 Kb region, including 40 hypothetical proteins and 6 IS family
229 transposases, among other genes. However, none of the genes comprised in such region seemed to be related
230 to sporulation (Supplementary Table 4). Furthermore, this variant had identical phenotypic traits to all other
231 selected variants.

232 **Reduced biofilm matrix production in mixed biofilms with the adapted variant**

233 The BT light variant phenotype showed increased CFU counts compared to the wild-type
234 phenotype after the eight-day evolution experiment, especially in biofilm settings (adhesion to slides).
235 However, the ancestral strain showed auto-aggregative phenotype in liquid cultures, unlike the variants,
236 suggesting a different pattern for the formation of cell aggregates (non-associated to a surface). We thus
237 wondered whether population size in biofilm settings may correlate with biofilm formation of the evolved
238 phenotype. We measured the total amount of biofilm formed (including cells and matrix) on the slides after
239 24 hours by quantification of crystal violet (CV) retention as an overall estimate of biofilm biomass. We
240 also quantified the specific prevalence of each strain by CFU counts of both the BT ancestral and V1 variant
241 strains (as shown in Figure 3). Biofilm biomass was similar for the BT ancestor and variant in mono-culture
242 while co-cultivation of ancestor and variant strains with PB, or in multispecies conditions, induced biofilm
243 biomass in both. However, when comparing mono-culture *vs.* mixed-culture conditions, such biomass
244 induction was only significant for the ancestral strain (Dunn´s post-hoc test, BT *vs.* BT+PB, $p = 0.0021$;
245 BT *vs.* BT+PD+PB, $p = 0.0106$; or V1 *vs.* V1+PB, $p = 0.0766$; V1 *vs.* V1+PD+PB, $p = 0.1104$; Figure 3a).
246 These results suggest differential adhesion or matrix production in mixed cultures. Mono- and co-culture

247 biofilms of variants V2, V3, and V6 reproduced the observed results for the ancestral and V1 variant strains,

248 indicating that the origin of the variants did not influence biofilm formation (Supplementary Figure 2a).

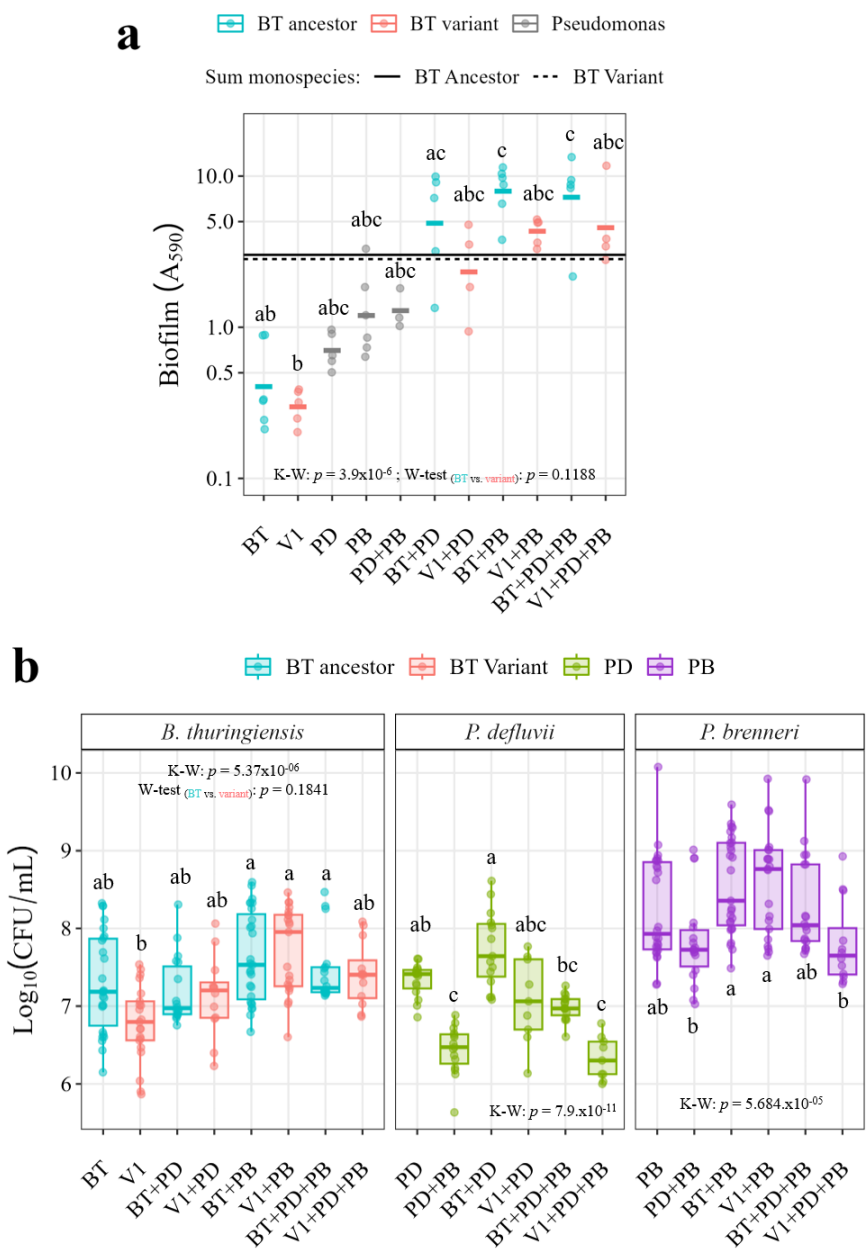

249

250 **Figure 3. Biofilm formation of *B. thuringiensis* ancestor, V1 variant and *Pseudomonas* in mono- or**
251 **mixed-species cultures after 24 h.** BT: *B. thuringiensis* ancestral strain (blue); V1: *B. thuringiensis* V1
252 variant (red); PD: *P.defluvii*; PB: *P.brenneri*. Adhesion was measured in mono-culture biofilms or in co-
253 culture with *P. defluvii*, *P. brenneri* or both (multispecies) in TSB medium after 24 h. K-W: significance of
254 a Kruskal-Wallis test, testing all combinations within each panel ($p < 0.05$). Dissimilar letters are indicative
255 of significant differences per panel, with $p < 0.05$ (Dunn´s post-hoc test). W-test$_{(BT\ vs.\ variant)}$: indicates
256 significance of a Wilcoxon´s rank sum test, comparing biomass (A_{590}) or CFUs based on BT phenotype.

257 **(a)** Mean biofilm measured as crystal violet stained biomass (A_{590}). Data based on ≥ 4 biological replicates,
258 represented as individual points. Each biological replicate consisted of 6 technical replicates. Horizontal
259 lines represent the predicted multispecies biofilm biomass, expected in case no biofilm induction or
260 reduction occur in co-cultures. This "predicted" value is derived from the sum of the monospecies biofilm
261 biomass by the constituent strains. **(b)** Biofilm CFU counts per mL of *B. thuringiensis, P. defluvii* and *P.*
262 *brenneri*. Data based on ≥ 9 biological replicates, represented as biological replicates, each consisting of ≥
263 3 technical replicates. Dissimilar letters show significance per species.
264
265 The CV results suggested differential adhesion or matrix production in mixed cultures with the
266 variant strain. Thus, we next quantified CFU counts for each strain in the different combinations to measure
267 specific adhesion. Cell counts of the BT ancestral and V1 variant strains within culture condition (i.e.,
268 monoculture, co-culture, or multispecies) were not significantly different (Dunn´s post-hoc test, Figure 3b,
269 left panel), indicating similar surface colonization for both strains. However, V1 cell numbers significantly
270 increased in co-culture with PB compared to mono-culture (V1 *vs.* V1+PB) (Dunn´s post-hoc test p =
271 2.06×10^{-05}, Figure 3b). Given that PB counts were unchanged despite the BT genotype, we hypothesize that
272 the adapted variant benefitted from co-cultivation with PB. CFU counts of the other variants replicated the
273 observations found for V1 in mono- and co-culture with PB (Supplementary Figure 2b).
274 In contrast, neither *Pseudomonas* species grew to a higher density in co-culture compared to mono-
275 culture conditions. Rather, PD experienced a reduction in cell counts when co-cultured with PB or in
276 multispecies biofilms with the variant phenotype, indicating an antagonistic effect of the adapted
277 phenotype, and PB, on PD cell numbers (Figure 3b).

278 To evaluate fitness of the ancestor and the V1 variant, we performed competition experiments that
279 included both strains, in the absence or presence of *Pseudomonas* spp. and in biofilm *vs.* planktonic settings.
280 We mimicked the selection pressure applied in a whole serial transfer during the adaptive evolution,
281 including co-cultivation, washing and regrowth in new media. The variant was significantly more abundant
282 under all conditions tested, except in biofilms in the absence of *Pseudomonas* (p = 0.064, Dunn's post-hoc
283 test; Figure 4). Interestingly, under biofilm settings, the ratio of variant to wild-type phenotype increased
284 from 4.8-fold to 25-48-fold when *Pseudomonas* spp. was present, highlighting the superior fitness of the
285 variant in the presence of other species (Figure 4, left panel).

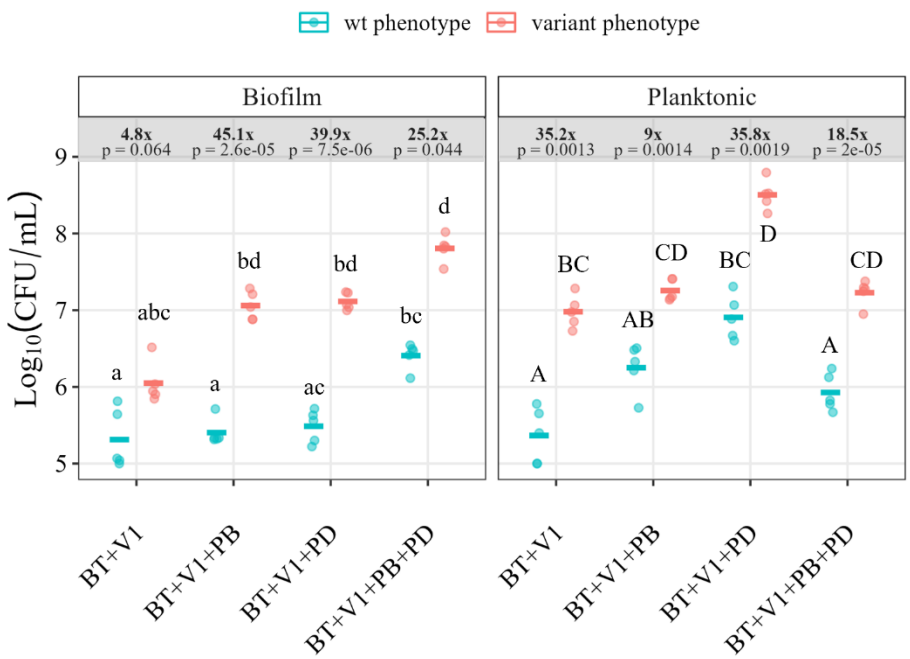

Figure 4. **Competition of *B. thuringiensis* ancestor and V1 variant under biofilms or planktonic settings, with or without *Pseudomonas* spp.** BT: *B. thuringiensis*; V1: BT V1 variant; PB: *P. brenneri*; PD: *P. defluvii*. Planktonic samples were cultivated for 24 h in TSB, diluted 1:1000 into fresh medium, and incubated for another 24 h before plating. Biofilm samples were cultured for 24 h, washed thrice, transferred to fresh media, and regrown for 24 h before plating. Plots show mean CFU counts (horizontal crossbars) of wild-type and variant colony phenotypes (Log_{10}(CFU/mL)). Data represent five biological replicates (points), each with three technical replicates. Dissimilar letters denote significant difference in multiple comparisons per combination ($p < 0.05$, Dunn's post-hoc test). Ratios of variant *vs.* wild-type phenotypes and their corresponding p-values (Dunn's post-hoc test) are shown in grey boxes for each sample type (culture condition) and setting (biofilm or planktonic).

Although the dynamics and ratios of wild-type and variant phenotypes varied in planktonic settings, prevalence of the variant phenotype was consistently enhanced in each mixture (Figure 4, right panel). These results confirm that the variant phenotype is fitter in the short term, not just after eight days of evolution, suggesting that it outcompetes the wild-type phenotype even early in the selection process. Furthermore, we evaluated the impact of the specific *Pseudomonas* spp. on the selection of variant or wild-type phenotypes in a triple culture system under both planktonic and biofilm settings. The abundance of the wild-type phenotype was significantly lower in biofilm settings compared to planktonic in the presence of PB, whereas abundance of the variant phenotype was unchanged (Two-sample t-test: $p$wt = 0.0119, $p$variant = 0.0923; Supplementary Figure 3a). In contrast, the abundance of both the wild-type and variant

306 phenotypes was enhanced in planktonic conditions compared to biofilms when PD was present (Two-
307 sample t-test: $p$wt =2.17x10^{-05}, $p$variant = 0.00794; Supplementary Figure S3b). These results suggest that
308 PD and PB interact differently with *B. thuringiensis*, which may result in different selective pressures posed
309 by the two *Pseudomonas* spp. Specifically, PD may facilitate nutrient availability or alter competition
310 dynamics in ways that favor planktonic growth of *B. thuringiensis*, regardless of its phenotype.
311 In conclusion, these findings suggest that the evolutionary adaptations in these variants may specifically
312 affect biofilm matrix production and aggregation without significantly impairing their ability to adhere to
313 surfaces. The observed reduction in matrix production in mixed-species biofilms with the variant could
314 stem either from the inability of *B. thuringiensis* light variant to induce matrix production in *Pseudomonas*
315 spp. or from intrinsic diminished matrix production in such variants.

316 **Matrix glycan composition altered by co-cultivation and BT light variant**

317 We observed a synergistic effect on biofilm biomass in mixed species, compared to mono-culture,
318 though only significantly different with BT ancestor (Figure 4a). However, no correlation was found
319 between such induction and CFU counts of either of the strains. We hypothesized that such differences in
320 biofilm biomass between ancestral and variant strains in mixed species might imply altered production of
321 biofilm matrix, either in BT variants or in the *Pseudomonas* species. Thus, we investigated the influence of
322 interspecies interactions and/or acquired mutations on the amount and types of glycans within the biofilm
323 matrix.

324 We screened multispecies biofilms (BT+PD+PB) with 78 different fluorescent lectins binding to
325 carbohydrates of varying nature (Supplementary Table 5). After filtering the binding results by fluorescence
326 signal (data not shown), three lectins with strong binding in multispecies biofilms were identified for further
327 analysis: AAL, WGA, and RCA. AAL binds α-fucose-containing polymers, WGA binds N-
328 acetylglucosamine (GlcNAc), and RCA binds galactose and N-acetylgalactosamine (Gal/GalNAc) glycans
329 [45]. Considering the minimal difference in biofilm biomass between co-culture and multispecies biofilms
330 (Figure 3a), we used co-culture conditions as it closely resembled multispecies conditions. Therefore, we

331 assessed binding of the three lectins to BT mono- and co-culture biofilms with PB, for both ancestral and
332 variant strains.

333 AAL lectin bound to BT cells and certain matrix-like structures in BT mono-culture biofilms, while
334 the variants displayed reduced lectin signal (Figure 5a). This indicates that the composition of
335 glycoconjugates in the cell wall or surface differed between the variants, leading to differential AAL
336 binding. Image quantification of lectin binding supported visual observations, significantly reducing lectin
337 binding in the variants (Figure 5b). However, the amount of lectin binding per biofilm volume (biovolume)
338 unit was not significantly changed in the variants (Figure 5c). We cannot exclude the possibility that
339 intrinsic heterogeneity of biofilm and differences among slide replicates, even within biological replicate,
340 could account for these results. Moreover, some of the replicates also showed some unspecific lectin
341 binding that could influence the analysis.

342 Co-cultivation of BT ancestral or variant strains with PB however showed similar AAL binding,
343 (Supplementary Figure 4), suggesting a change in glycoconjugates triggered by interspecies interactions.
344 Moreover, PB also showed AAL binding in mono-culture and, thus, association of lectin signal with the
345 specific matrix producer may be cumbersome in co-culture conditions (Supplementary Figure 4, BT and
346 PB panels).

347 Unlike AAL lectin binding, no differential binding was observed for RCA lectin, regardless of the
348 BT genotype or cultivation (mono- *vs.* co-culture with PB). Moreover, in PB biofilms, this lectin bound
349 thin filaments that revealed a galactose/N-Acetylgalactosamine polymer network (Supplementary Figure
350 5a). On the other hand, WGA bound to BT cell surfaces (Supplementary Figure 5b), likely the cell wall
351 because this lectin binds to the sugar GlcNAc, which is a major component of peptidoglycan [46]. However,
352 there was no visible difference observed in either the variants or mixed-species combinations (data not
353 shown).

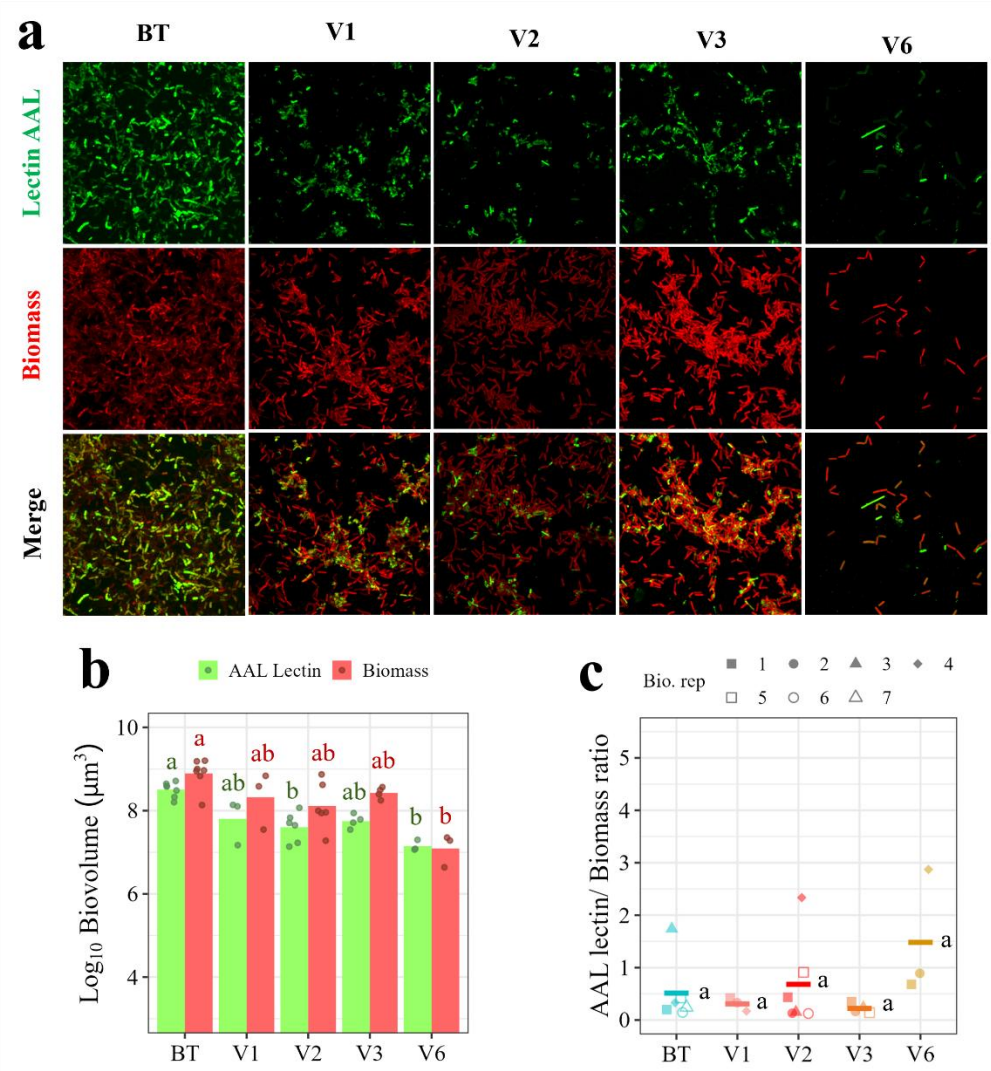

Figure 5. AAL lectin staining in mono-culture biofilms of *B. thuringiensis* ancestor and variant strains. BT: Ancestral *B. thuringiensis* strain; V1: variant1, V2: variant 2; V3: variant 3; V4: variant 4; PB: *P. brenneri*. Biomass: red fluorescent signal of biofilms stained with the cell biomass stain SYTO60. Lectin AAL: green fluorescent signal of biofilms stained with the fluorescent lectin AAL-FITC. Merge: combined fluorescent signal of cell biomass and lectin stains. **(a)** Maximum intensity projection (MIP) images of Z-stacks recorded by confocal laser scanning microscopy for 24-hour biofilms. The scale of the images is 124 µm across. **(b)** Biofilm volume (Biovolume, μm^3) of lectin (green) and cell biomass fluorescence (red). Biovolume was calculated using BiofilmQ [86] per channel, based on ≥ three biological replicates (represented as points) and two images per replicate. Bars show mean values per channel. Dissimilar letters denote significant p-value (Dunn´s post-hoc test, $p < 0.05$) per channel (green = lectin; red = cell biomass). **(c)** Ratios of lectin biovolume/ biomass biovolume for each strain. Data based on ≥ three biological replicates, represented by different symbols, and two images per replicate. Crossbars indicate the mean ratio for each strain. Dissimilar letters denote significant p-value (Dunn´s post-hoc test, $p < 0.05$).

368 In conclusion, AAL lectin staining showed a tendency of reduced production of α-fucose polymers
369 by BT variants but lectin-biomass ratios were not conclusive. However, other matrix components may be
370 influenced by the distinct phenotypic biofilm formation by BT genotype, such as protein abundance.

371 **Matrix protein abundance of BT light variant decreased in response to co-cultivation and genotype**

372 We next investigated the effects of interspecies interactions and acquired mutations in BT on the
373 proteomes of biofilm matrices, hoping to explain the reduced biofilm matrix production observed in either
374 the BT variants or the *Pseudomonas* species. We specifically examined variants V1 and V6 due to their
375 distinct origin of isolation (V1 from co-culture with PB and V6 from mono-culture), to eliminate the
376 possibility that the isolation origin influenced the abundance of matrix proteins. Our proteomic experiments
377 utilized a chemical extraction of biofilm matrix as input material, which results in a lower number of
378 expected proteins compared to total biofilm samples.

379 First, we performed a comparative analysis of BT proteomes by genotype (variants *vs*. ancestral
380 strains) and culture condition (mono-culture *vs.* co-culture with PB) (Figure 6). It is important to note that
381 co-culture proteomes likely contain BT and PB derived proteins from the extracted matrices. The analysis
382 showed that BT ancestor mono-culture samples were the most distinct from the rest, clustering together on
383 the right of PC1 (Figure 6a), as evidenced by probabilistic principal component analysis (PPCA). The
384 variation in PC1 was driven by the BT genotype (ancestor *vs.* variant), while the cultivation condition
385 (mono-culture *vs.* co-culture) determined PC2. Light variant co-culture or mono-culture samples could not
386 be discriminated, while BT ancestor co-culture samples were grouped in a distinct cluster compared to
387 mono-culture. Interestingly, BT co-culture proteomes overlapped with variant mono- and co-culture
388 proteomes. Consistently, comparison of BT ancestor *vs.* variants in mono-culture evidenced the largest
389 difference in proteomes. Only 20 proteins out of 187 were common to all three BT strains (Figure 6c and
390 Supplementary Table 6) and 11 significantly changed, related to amino acid and carbohydrate metabolism
391 energy production, among others. In contrast, 150 proteins were exclusively detected in the ancestor
392 (Supplementary Table 7), indicating a major reduction in protein abundance in both variants. Among those,

different proteins involved in sporulation or regulated by the Stage 0 sporulation protein, Spo0A, were only detected in the ancestor, consistent with sporulation-defective phenotypes observed in the variants.

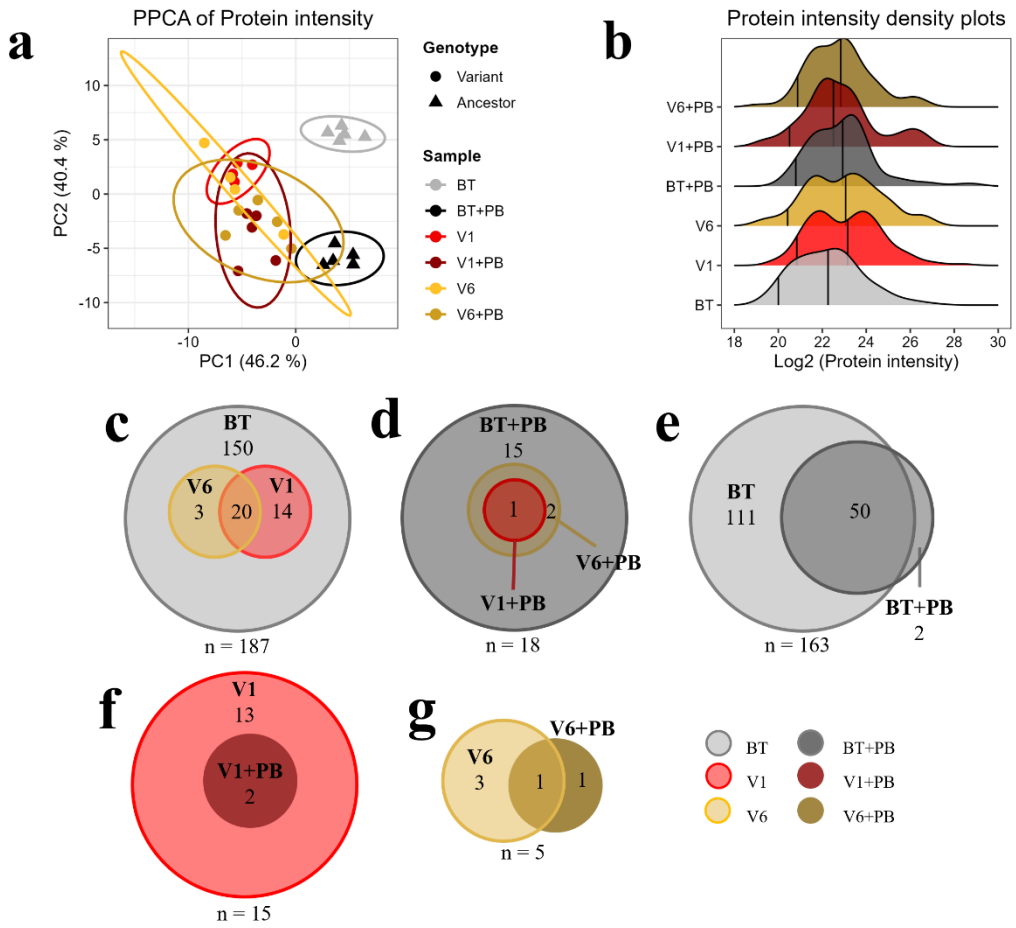

Figure 6. Differential protein abundance in *B. thuringiensis* ancestor *or variants* in mono-culture *vs.* co-culture biofilms with *P. brenneri*. BT = Ancestral *B. thuringiensis* strain; PB = *P. brenneri*; V1 = *B. thuringiensis* variant 1; V6 = *B. thuringiensis* variant 6. **(a)** Probabilistic PCA plot of all monoculture and co-culture proteomes, based on Log_2 transformed protein intensity data with 5 biological replicates per sample. Color indicates the sample type (strain and culture condition) and shape the genotype: ancestral (triangles) or variant (circles). Ellipses indicate sample group clustering based on the principal components. **(b)** Density plots of Log_2 transformed protein intensity for mono-culture *vs.* co-culture samples representing 5 biological replicates. Percentile 0.05 is indicated as the leftmost vertical line, while middle lines denote protein intensity means for each sample excluding NA values (no protein detected). **(c-g)** Venn diagrams of *B. thuringiensis* mono-culture proteomes (c), co-culture proteomes (d), or mono-culture *vs.* co-culture proteomes (e-f), considering proteins detected in ≥ 60 % of each sample (3/5 biological replicates). **(c)** Mono-culture proteomes **(d)** Co-culture proteomes **(e)** BT *vs.* BT+PB proteomes **(f)** V1 *vs.* V1+PB proteomes **(g)** V6 *vs.* V6+PB proteomes. n = total proteins detected per comparison.

To discard unique expressions due to detection limits, we calculated the mean and 0.05 percentile of each proteome to use as a cutoff (Figure 6b and Supplementary Table 8). However, DivIVA, SpoVG,

411 immune inhibitor A (CDS_04360 and CDS_05099), neutral protease B (CDS_00401) and the major biofilm
412 matrix component TasA(CDS_04363 and CDS_04365) were still above the expression cutoff in the
413 ancestral BT strain, compared to the light variants. Remarkably, the four latter proteins were also more
414 abundant in the ancestral co-culture (Supplementary Table 9), suggesting that their abundance is influenced
415 by BT genotype —ancestor — and the presence of PB.

416 Co-cultivation of PB with BT ancestral or variant strains reduced biofilm matrix protein abundance
417 by 90 % (17 proteins co-culture *vs.* 187 in mono-culture), suggesting that PB minimized the differences of
418 BT proteomes (Figure 6d). However, 15 proteins were uniquely detected in the ancestor co-culture,
419 including the four mentioned above (Supplementary Table 9). Mono-culture *vs.* co-culture comparisons
420 rendered highly different results depending on the genotype compared. In the ancestor pairwise analysis,
421 111 out of 163 proteins were only detected in mono-culture (Figure 6e and Supplementary Table 10),
422 supporting the previous observation that PB decreased abundance of biofilm matrix-associated proteins in
423 BT. However, comparisons between the V1 and V6 variants resulted in reduced matrix proteomes, with 15
424 and 5 proteins detected, respectively (Figures 6f-g and Supplementary Tables 11-12). Importantly, these
425 findings reflect the proteomes of extracted matrices rather than global proteomes, as we would anticipate a
426 broader range of differentially abundant proteins in global proteomes due to *spo0A* mutations, considering
427 its pivotal regulatory role.

428 We hypothesize that the acquired mutations may switch off the expression of multiple genes
429 involved in sporulation, a highly complex and tiered-regulated process linked to biofilm formation. There
430 is previous evidence that *spo0A* mutations in *Bacillus subtilis* enhanced maintenance metabolism [47] and
431 increased glucose consumption and acetate formation [48]. This would be consistent with the faster
432 doubling time observed for the variants, given that fewer proteins and consequently a lower amount of
433 energy are required in the absence of sporulation.

434 We investigated whether matrix proteins were differentially abundant in PB based on culture
435 condition and BT genotype (Supplementary Figure 6). Out of 169 detected proteins, mono- and co-culture
436 proteomes showed similar mean abundance and 0.05 quantiles (Supplementary Table 8 and Supplementary

437 Figure 6a). Unlike BT results, co-cultivation did not strongly affect the number of detected proteins, with
438 64% shared among all samples (n = 108) (Supplementary Table 13 and Supplementary Figure 6b). PB
439 mono-culture samples clustered separately to co-culture samples, indicating that cultivation drove PC1
440 (Supplementary Figure 6c). Seventeen proteins were uniquely detected in co-culture with BT ancestor
441 (Supplementary Table 13), though co-culture samples of BT, V1, or V6 could not be discriminated in the
442 PPCA. While no unique or differentially abundant matrix proteins were found in PB, multiple proteins
443 involved in amino acid transport and metabolism varied based on culture condition. Co-cultivation reduced
444 the abundance of several amino acid transporters in PB regardless of BT genotype (arginine, branched-
445 chain, cysteine, glutamate/aspartate, and putrescine, Supplementary Figure 6d). Other proteins involved in
446 branched-changed transport (braC_1), glycine, tyrosine or arginine/ornithine metabolism were only
447 detected in PB monoculture (Supplementary Table 13). These findings suggest that PB optimizes amino
448 acid utilization differently depending on environmental conditions. In co-culture with BT, ecological
449 dynamics might shift, altering metabolic priorities and protein abundance. This aligns with our previous
450 observation that V1 variant CFU counts increased in co-culture with PB, suggesting that the variant benefits
451 more from co-cultivation with PB than the ancestral strain (Figure 4b).

452 Based on all proteomics results, we hypothesize that the lower abundance of matrix-associated
453 proteins in BT light variants correlates with the previously observed reduction in biofilm biomass in the
454 variant mixtures. Furthermore, the absence of differential or unique abundance of matrix proteins in PB
455 suggests a deficiency in BT's production of matrix components associated with *spo0A* mutations. These
456 results are also consistent with the observed tendency of reduced AAL lectin binding in the variants.

457 # Discussion

458 Microbial interactions influence the fitness, survival, and evolution of interacting species, enabling
459 better resource utilization, mitigating competition, enhancing mutual dependencies, or optimizing nutrient
460 exchange. Despite their predominance and significance, adaptive evolution experiments focusing on
461 multispecies biofilms remain limited. This study aimed to address this gap by examining effects of
462 interspecies dynamics and spatial structuring on trait selection within the Gram-positive bacterium BT.

463 Here, we used short-term evolution assays where BT, PD, and PB were cultured individually or in
464 combination, under both planktonic and biofilm conditions (Figure 1a). Throughout, these assays, a distinct
465 phenotypic variant of BT, which we termed "light variant", consistently emerged. Notably, this variant was
466 more prevalent than the wild-type phenotype in biofilm environments (Figure 1b), and its selection further
467 amplified by interactions with *Pseudomonas* species—indicating a potentially fitter phenotype under such
468 conditions. While previous experimental evolution studies in biofilms have documented the emergence of
469 adapted variants exhibiting enhanced biofilm characteristics relative to their ancestors, our findings diverge
470 [18, 20, 49, 50]. For instance, Lin and collaborators identified a "fuzzy spreader" phenotype of *B.*
471 *thuringiensis* in a bead-transfer evolution study, where all adapted lineages resulted in enhanced biofilm
472 production compared to its ancestor [26]. In contrast, the BT variants identified in our study produced less
473 biofilm within mixed-species contexts, which was associated with a reduction in biofilm matrix components
474 like TasA. Despite this, the adapted phenotype prevailed across different environments (planktonic or
475 biofilm, Fig. 1b), suggesting a fitness advantage over the ancestral form. Moreover, the adapted variant
476 displayed reduced auto-aggregation compared to the ancestral strain (Figure 2a-b). This decrease in
477 aggregation could optimize the distribution of cells within the environment, facilitating better access to
478 nutrients and, possibly, enhancing survival and growth. This advantage is consistent with the observed
479 shorter generation time of the non-sporulating variants and higher prevalence of the light variant V1 when
480 co-cultured with the ancestor, especially in the presence of other species (Figure 4). These traits together
481 would confer a substantial fitness benefit, especially in competitive environments with other species, where

482 the ability to outcompete other organisms and rapidly access resources could be crucial for survival and
483 proliferation (Figure 7). However, considering the comparable biofilm characteristics between the ancestor
484 and the variants, our findings suggest that BT adaptation in biofilms may be driven by factors beyond
485 adhesion or biofilm formation, such as nutrient competition and subsequent metabolic optimization, which
486 may also be more compatible with *Pseudomonas* co-existence.

487 Biofilm formation and spore production are two different survival strategies of bacteria facing
488 adverse environmental stresses. However, intertwined regulatory pathways between biofilm formation and
489 sporulation have been proposed for both *B. subtilis* and *Bacillus cereus* [51, 52]. *spo0A* mutants in other
490 *Bacilli* such as *Bacillus velezensis*, *B. subtilis* or *B. cereus* are impaired in biofilm formation, since Spo0A
491 de-represses EPS production and promotes biofilm [53–56]. Whole-genome sequencing of the variants
492 linked lack of sporulation with mutations in key genes regulating sporulation (Supplementary Figure 1).
493 V1, V3 and V6 variants harbored mutations in *spo0A*, which has a central role in sporulation [41, 42].
494 However, BT variants lacking Spo0A showed comparable CFU counts and matrix production to the
495 ancestor in mono-culture (Figure 3). Our results demonstrate that, even though the variant displayed
496 reduced capacity for auto-aggregation (surface-independent aggregation), it does not entirely lose the ability
497 to attach to surfaces, distinguishing it from other *spo0A* mutants in Bacilli such as *B. subtilis* and *B. cereus*.
498 On the other hand, V2 variant showed structural variation (SV) affecting the *soj* gene. SV can confer change
499 in gene copy number, creation of new genes, altered gene expression and many other functional
500 consequences [57]. Other studies have demonstrated that certain mutations creating structural variants can
501 enable new adaptive phenotypes to arise in laboratory populations of microorganisms, that may be
502 inaccessible single-nucleotide mutations [43, 58]. Soj has been associated to correct chromosome
503 segregation and partitioning during both growth and initiation of sporulation in *B. subtilis* [44]. The
504 regulation of chromosome structure by Soj is particularly important during sporulation, when the bacterial
505 cell undergoes significant changes in chromosome architecture. Thus, structural variation affecting this
506 gene may explain the non-sporulating phenotype of this variant.

507 A recent study established a link between spore formation and biofilm dispersal in *B. subtilis* [59].
508 Under unfavorable conditions, spores may detach from the biofilm, dispersing through air, water, or other
509 means, and potentially establishing new biofilms elsewhere, thereby promoting bacterial survival and
510 spread. Our findings indicate that, under the controlled conditions of the laboratory where environmental
511 stressors are minimal or absent, sporulation might become dispensable for BT (Figure 7). However, non-
512 sporulating variants have also been reported in other Bacilli in more relevant ecological contexts, such as
513 deep nutrient or energy deprivation, food surfaces or insect cadavers, where they survived from days to
514 months [60–62]. This suggests that our findings can have ecological relevance and that such mutations can
515 be selected and fit in more extreme conditions.

516 Irrespective of the specific mutations, all BT light variants shared identical phenotypic traits: grew
517 faster than the ancestor (Supplementary Table 3), displayed reduced auto-aggregation (Figure 2a-b), did
518 not sporulate (Figure 2c), and bound the AAL lectin less, which pointed towards decreased matrix
519 glycoconjugates (Figure 5). Moreover, proteomic analysis revealed that different matrix proteins were
520 uniquely detected in the ancestor. Among these, two TasA/CalY orthologues and SpoVG were detected in
521 BT ancestor but not in the variants (Supplementary Table 7). TasA is a major matrix component in *Bacillus*
522 biofilms and its absence results in significant defects in biofilm and pellicle formation in *B. subtilis* [63,
523 64]. Its paralog in *B. cereus* is needed for root colonization, while in *B. thuringiensis*, the TasA-orthologue
524 CalY has been identified as a cell-surface adhesin and described as a major virulence factor and biofilm
525 matrix protein [65, 66]. Interestingly, both CalY orthologues (*tasA_3* and *tasA_4*) are located in the same
526 operon as *sipW*, regulated by SinR and, consequently, indirectly controlled by Spo0A in *B. cereus*
527 (Supplementary Figure 7). Such regulatory circuit would explain the lack of TasA in *spo0A*-deficient
528 variants. On the other hand, SpoVG plays a critical role in the spore-coat formation of *Bacillus anthracis*
529 and is a regulator of both sporulation and biofilm formation in *B. cereus* 0-9 that activates the levels of
530 Spo0A and, thus, the fate of *B. cereus* cells: biofilm or sporulation [67–69]. Proteomic results also
531 evidenced the unique detection of two metalloproteases only in BT ancestor: NprB and InhA (immune
532 inhibitor A), linked with protein recycling during sporulation and indirectly regulated by Spo0A [41, 70,

533 71]. InhA coding gene, *ina_4*, is also located in the same genomic region than the two *calY* orthologues and
534 regulated by the SinI-R regulon in other Bacilli [72, 73]. We speculate that the lack of expression of TasA
535 and the biofilm regulatory protein SpoVG could contribute to the differences observed between CFU counts
536 and total biofilm biomass for the variant phenotype (Crystal Violet).

537 Apart from BT genotype, co-cultivation was another factor influencing protein abundance, yet
538 differently depending on the target species. Co-cultivation significantly altered the proteome of BT but only
539 in the ancestral strain (Figure 6a). Meanwhile, for PB the presence of BT greatly impacted protein
540 abundance regardless of the phenotype (Supplementary Figure 6c), showing consistent lower abundance of
541 amino acid transporters in PB co-culture (Supplementary Figure 6d). This could indicate competition for
542 resources or utilization or distinct metabolic pathways in co-culture. We have previously reported that
543 cooperative interactions between community members can facilitate metabolic cross-feeding on specific
544 amino acids, though in a different multispecies biofilm model [74, 75]. Additionally, previous studies have
545 shown that coexistence can remain stable over time, for instance, by oppositely altering the pH or secreting
546 costless by-products to the other species' benefit [18, 76–80]. Most reported *Bacillus-Pseudomonas* co-
547 cultures demonstrate either competition or amensalism, driven by bioactive natural products, while positive
548 interactions are usually associated with cross-feeding or shared resources [31]. Our evolution experiment
549 revealed significant reduction of PB CFU counts in planktonic co-culture with BT, unlike biofilm
550 conditions, suggesting that spatial structure facilitates co-existence of these species. Furthermore, higher
551 abundance of the variant phenotype was observed in co-culture with PB in both planktonic and biofilm
552 settings, suggesting that the adapted variant benefits from PB, compared to its ancestor. This pattern is
553 consistent with a non-exploitable dynamic, with the BT variant benefiting through improved growth
554 without negatively impacting PB.

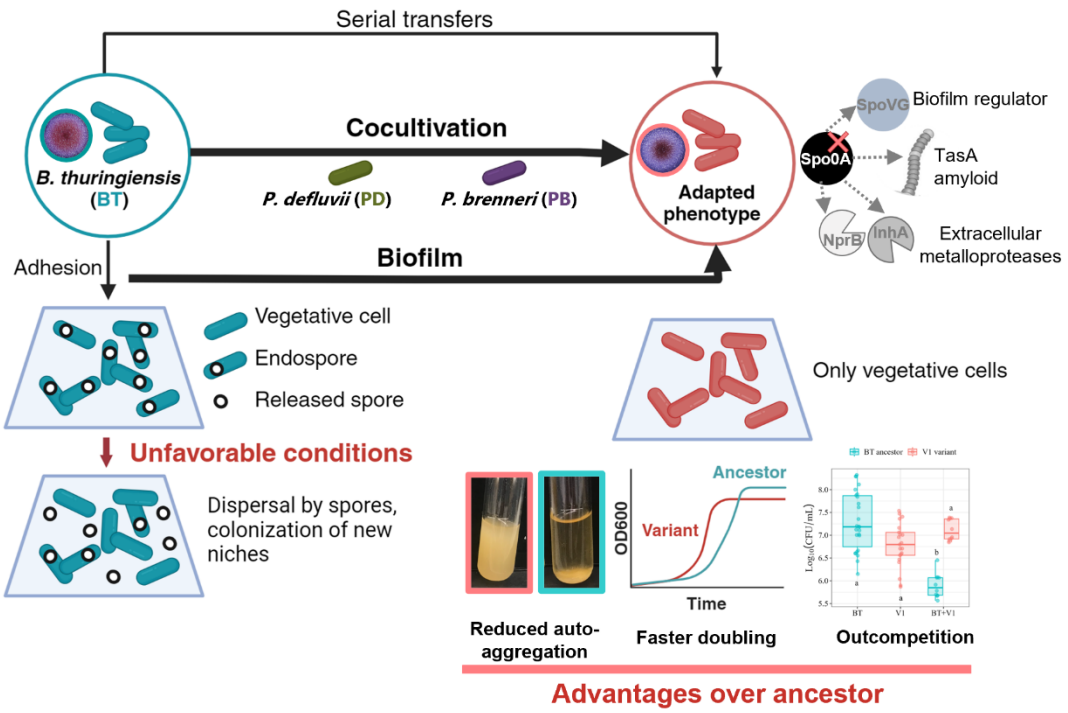

Figure 7. Proposed model for adaptation of the evolved variants. *B. thuringiensis* non-sporulating variants emerged in all conditions, but biofilm settings and co-cultivation with either or both *P. brenneri* and *P. defluvii* enhanced selection of the variant (thicker arrows). In adverse conditions, spores might aid in dispersing biofilms in the ancestral strain. However, adapted variants, lacking sporulation, could experience restricted dispersal. The adapted variant lacks sporulation, displays reduced auto-aggregation, faster doubling time than its ancestor and can outcompete it in co-culture biofilms. Variants lack proteins SpoVG, the matrix amyloid TasA and two extracellular metalloproteases involved in matrix recycling. Indirect Spo0A regulation is indicated by dashed arrows [41, 54, 67, 68, 73, 99].

In summary, our study evidences the ecological role of non-sporulating variants of *B. thuringiensis* in multispecies communities, demonstrating that prevalence of the variant phenotype is likely influenced by its lower auto-aggregation capacity, its competitive advantage in the presence of *Pseudomonas* spp. and its ability to thrive in both planktonic and biofilm environments (Figure 7). However, our results showed enhanced prevalence of the variant phenotype over the wild type in biofilm settings and in the presence of *Pseudomonas* species, suggesting that selection of the non-sporulating variants is strongly influenced by such factors (Figure 7). Our findings challenge the traditional view that biofilm evolution invariably selects for stronger biofilm-forming phenotypes. Instead, we demonstrate that adaptation may favor traits that optimize resource competition or metabolic efficiency over biofilm reinforcement. These results have

573 important ecological implications, as similar evolutionary dynamics may occur in natural microbial
574 communities where competition and cooperation among species influence community structure. Hence,
575 this study evidences the importance of considering population diversity—both intra- and interspecific, along
576 with spatial structure as key determinants of bacterial adaptation.

577 # Methods

578 **Strains and materials**

579 The three bacterial strains PD, PB, BT were isolated from water samples collected at a wastewater
580 treatment plant in Kalundborg, Denmark, and their genome s were sequenced in another study [29]. All
581 strains were grown at 24 °C in Tryptic Soy Broth (TSB; 17 g pancreatic digest of casein, 3 g papaic digest
582 of soybean meal, 5 g sodium chloride, 2.5 g dextrose, 2.5 g dibasic potassium phosphate in 1 L distilled
583 water, pH 7.3), supplemented with 1.5 % agar when needed. To distinguish the bacterial strains and/or
584 species variants, 40 µg/mL of Congo Red (Merck) and 20 µg/mL Coomassie Brilliant Blue G (Sigma-
585 Aldrich) were added to the TSB base, referred to as TSB Congo Red plates. In previous studies, this media
586 has facilitated identification of adapted variants and differentiation among species [18, 77].

587 **Short-term evolution assay with spatial structure**

588 Overnight cultures in TSB medium were adjusted to an optical density at 600 nm (OD_{600}) of 0.15
589 in fresh TSB prior to usage. The experiment was conducted in 24-well plates, where each well contained a
590 polycarbonate chip (12 x 12 x 0.78 mm^3) (PC) that was diagonally tilted so that bacteria could adhere to
591 both sides of the chip. In each well, 2 mL of OD_{600} 0.15 cultures were added, either as mono-species culture
592 or mixed-species culture. For mixed-species conditions, 1:1 or 1:1:1 OD_{600} ratios of the species were used,
593 that is, 1 mL or 0.66 mL of each species at OD = 0.15, for dual- and multispecies, respectively. Every 24
594 hours (h), the floating pellicle was gently removed and discarded before the polycarbonate chip, containing
595 adhered cells, was transferred to a new well, and the chip was washed thrice in 1x phosphate-buffered saline
596 (PBS) to remove any leftover planktonic/pellicle cells. This was done consecutively for 8 days, followed
597 by washing the PC chips before transferring to a 5-mL Eppendorf tube containing 2 mL 1x PBS. The biofilm
598 was then removed from the PC surface by shaking at 600 rpm for 5 minutes (min) (Titramax1000,
599 Heidolph). The resulting suspension was then plated on TSB Congo Red plates with three technical
600 replicates to estimate colony forming units (CFUs) and to screen for new variants with different colony
601 morphology.

602 **Short-term evolution assay without spatial structure**

603 To test selection pressure in conditions not favoring spatial structure, a short-term evolution assay
604 was also performed with well-mixed planktonic cultures. Cultures were adjusted to OD_{600} = 0.15 as
605 described above, and 5 mL of this culture was incubated overnight, with shaking at 250 rpm (KS 250 basic,
606 IKA). After 24 h, 5 µL of this culture was transferred to new fresh media. The transfer was repeated for 8
607 days, followed by plating on TSB Congo Red plates with three technical replicates.

608 **Sedimentation dynamics in planktonic cultures of BT ancestor and V1 variant**

609 The sedimentation dynamics of the BT ancestor and V1 variant strains were assessed in planktonic
610 cultures grown in TSB at 24 °C and 250 rpm for 20 h. A 1-mL aliquot of each strain culture was transferred
611 to a spectrophotometer cuvette. Culture aliquots were maintained under static conditions to observe natural
612 sedimentation patterns. OD_{600} was measured at time zero (t0) and for 60 minutes (min) in 5 min intervals
613 using a GENESYS UV10 spectrophotometer (Thermo Scientific), to quantify sedimentation. Values were
614 expressed as the percentage of initial OD_{600} (t0). Measurements were performed for three biological
615 replicates of each strain, and mean percentage of initial OD_{600} calculated per time point.

616 **Microscopic analysis of auto-aggregation in planktonic cultures of BT ancestor and V1 variant**

617 The auto-aggregative properties of the BT ancestor and V1 variant strains were analyzed using
618 fluorescence microscopy. Planktonic cultures of both strains were grown in 5 mL TSB for 20 h at 24 °C
619 and 250 rpm. Cultures were left for 1 h without shaking and 20 µL of top or bottom phases stained with 10
620 µM SYTO 16 (nucleic acid stain) to visualize cellular distribution. Images of the top and bottom phases of
621 the cultures were captured using a Zeiss Axio Observer Z1 epifluorescence microscope equipped with a
622 LD Plan-NEOFLUAR 20x objective (numerical aperture 0.4).

623 **Quantification of biofilm formation**

624 Assessment of the biofilm formation on the polycarbonate surfaces was performed using a modified
625 crystal violet (CV) assay [81]. Biofilms were allowed to grow on PC chips for 24 h as described above,
626 washed thrice in 1x PBS and then transferred to a well of a 24-well plate containing 2 mL of 1 % CV
627 aqueous solution and incubated for 20 min in the dark. Then, the chips were carefully removed and rinsed
628 five times in 1x PBS. CV-stained chips were then incubated in 2 mL of 96 % ethanol for 30 min. The
629 biofilm biomass was then quantified as the absorbance of CV solution at 590 nm (A_{590}). To avoid
630 measurement saturation, samples were diluted in 96% ethanol when A_{590} was higher than 1.

631 **Growth curves in liquid cultures**

632 Cultures of BT strains were grown overnight in liquid TSB medium. Then, 1:100 dilutions of the
633 overnight cultures in TSB were prepared, and these cultures were used to inoculate 96-well plates, using 3
634 biological and 3 technical replicates. Growth was monitored for 24 h at 24 °C with 282 rpm double orbital
635 shaking and OD_{600} readings every 10 min. Growth data was integrated to calculate different growth
636 parameters using the Growthcurver R package [82] to determine different parameters. These included:
637 t_mid, the point of inflection of the growth curve; K, carrying capacity or maximum size of the population;
638 t_gen, generation time of a strain; r, intrinsic growth rate of a population; sigma, the fit goodness of the
639 model. The resulting calculations can be found in Supplementary Table 3.

640 **Whole-genome sequencing and analysis of variants**

641 BT ancestor and isolated variants V1, V2, V3, and V6 (Supplementary Table 2) were genome-
642 sequenced by extracting the DNA using DNeasy Blood & Tissue Kit (Qiagen) from overnight cultures. The
643 samples were sequenced with short reads using Truseq libraries on the Illumina NovaSeq 6000 and 2x150
644 cycles (Novogene, UK).

645 Data was analyzed using breseq (v0.35.0) to call variants using the –p polymorphism flag when
646 analyzing population sequences [83]. As the reference genome, we used the previously constructed hybrid

647 assembly of long and short reads from BT, available online (NCBI) with ID JARTVI000000000. Mutations
648 detected between our ancestral strain and the reference genome were not considered. The breseq software
649 also predicts new junctions within the genome which may occur due to mobile element insertions, large
650 deletions, structural rearrangements and prophage excision. These analyses were also included. A full list
651 of the mutations can be found in Supplementary Table 4.

652 **Optical microscopy**

653 Liquid cultures of the different strains were incubated for 24 h in TSB at 24 °C while shaking at
654 250 rpm. From these 24-h cultures, 10 µl were pipetted onto a microscope glass slide, and a coverslip was
655 applied on top. Samples were observed with an Olympus BH2 optical microscope with 10x and 40x
656 magnification objectives, with 0.25 and 0.65 numerical apertures, respectively.

657 **Sporulation assay**

658 To compare the sporulation capacity of *B. thuringiensis* and its variants, a sporulation assay was
659 performed similarly to the description by Toukabri et al. [84]. Firstly, overnight cultures (24 h) of the
660 ancestor and variants were serially diluted and plated on TSB Congo Red to quantify the concentration
661 vegetative cells in each culture. Similarly, an aliquot of such cultures was heat-shocked at 80 ˚C for 20 min
662 before plating on TSB Congo Red plates to quantify sporulating cells. Plates were incubated two days at
663 24 ˚C before counting. This was repeated for 3 consecutive days (48-, 72- and 96-h cultures) to assess
664 whether incubation time influenced spore formation. Furthermore, the sporulation assay was performed for
665 the biofilms grown on PC chips to estimate the number of spores produced in mono or mixed-species
666 cultures.

667 **Competition assay of BT ancestor and V1 variant in biofilm and planktonic settings with or without**
668 ***Pseudomonas* spp.**

669 To assess fitness of the ancestral BT and V1 variant, they were grown in the absence or presence
670 of *Pseudomonas* spp. under planktonic or biofilm conditions simulating a full serial transfer of the evolution

experiment. Overnight cultures of each strain were adjusted to OD_{600} = 0.15 in fresh TSB and mixed in equal volume ratios: 1:1 (BT+V1), 1:1:1 (BT+V1+PB; BT+V1+PD) and 1:1:1:1 (BT+V1+PB+PD).

Inoculation of biofilm and planktonic samples was done as detailed in the short-term evolution assay with and without spatial structure, respectively, however with only one daily transfer. Specifically, planktonic samples were cultivated in TSB for 24 h at 24 °C and 250 rpm, diluted 1:1000 in fresh medium and incubated for another 24 h before plating. For biofilm samples, they were cultivated in TSB for 24 h at 24 °C under static conditions, washed three times with fresh medium, transferred to new media, and regrown for another 24 hours before plating. Colony-forming unit (CFU) counts of BT ancestor and the V1 variant were determined by plating and counting on TSA Congo Red. Each condition included five biological replicates, with each replicate consisting of three technical replicates.

Biofilm matrix staining with fluorescent lectins

Matrix glycoconjugate characterization in the three species community was performed using 78 different fluorescently labeled lectins (using FITC, AlexaFluor488, or Fluorescein) in combination with confocal laser scanning microscopy (TCS SP5X, Leica Germany, controlled by the software program LAS-AF vers. 2.41) as described previously by Neu and Kuhlicke [45, 85]. The lectins and fluorescent conjugates used are listed in Supplementary Table 5. Briefly, biofilms were grown on polycarbonate chips for 24 h, followed by washing three times with 1x PBS, as described above. Staining solutions containing fluorescent lectins were prepared at a concentration of 100 µg/mL (in filter-sterilized ultrapure water). 100 µL was then added to a biofilm on a polycarbonate chip, followed by incubation for 30 min in the dark. The excess staining solution was washed twice with dH_2O before adding SYTO60 to the sample, prior to confocal imaging. Excitation of FITC, AlexaFluor488, and Fluorescein was performed at 488 nm, and the emission signals were recorded from 500–580 nm. Excitation of SYTO60 was at 652 nm, and emission was recorded from 665-750 nm. For lectins conjugated to Rhodamine, excitation was done at 525 nm, and emission was recorded from 570-650 nm. Image data sets were recorded using 63x NA 0.9 and 63x NA 1.2 objective lenses with a step size of 0.5 µm.

696 Based on the screening, three lectins, *Aleuria aurantia* Lectin (AAL), Wheat Germ Agglutinin
697 (WGA), and *Ricinus communis* Agglutinin (RCA), were chosen for further testing. Here, monospecies and
698 dual species biofilms of PB and BT ancestral or variant strains were used to better assess the effects of BT
699 genotype and co-cultivation on AAL lectin binding. Images of AAL-lectin-stained biofilms of BT,variants
700 V1, V2, V3 and V6 strains were analyzed using the biofilm image analysis software suite BiofilmQ [86].
701 Biofilm volume (biovolume) was calculated for each fluorescent channel: lectin (FITC channel) and
702 biomass (SYTO60 channel) with a minimum of 6 images per sample (3 biological replicates and 2 images
703 per replicate). Moreover, biovolume ratios (AAL-lectin-stained biovolume divided by the total biovolume)
704 were calculated per image.

705 **Biofilm matrix proteome measurements**

706 Mono-cultures and co-culture biofilms were grown for 24 h in TSB medium on PC chips as
707 described above, followed by washing 3 times in 1x PBS to remove planktonic cells and biofilm pellicle.
708 Five biological replicates per condition were processed, each composed of five PC chips that were
709 combined to extract enough biofilm matrix material for proteomics analysis (technical replicates). The
710 biofilm was then resuspended in 5 mL of 1x PBS by shaking at 1000 rpm for 10 min. The biofilm matrix
711 was extracted from biofilms grown in either mono-culture or co-culture, resulting in a mixture of matrix
712 components from both species, by the formaldehyde and NaOH extraction method [87, 88]. Briefly, 0.006
713 V formaldehyde 37 % (30 µl) was added to the biofilm samples and incubated for 1 h at 4 °C while mixing,
714 followed by addition of 0.4 V NaOH 1 N (2 mL) and incubation for 3 h at 4 °C while mixing. Samples were
715 then dialyzed using 3500 MWCO 22 mm SnakeSkin™ Dialysis Tubing (ThermoFisher Scientific) against
716 2.5 l milliQ water, overnight at 4 °C with stirring. Protein content in dialyzed samples was quantified using
717 the Bio-Rad Protein assay, a modified Bradford assay [89], before freezing with liquid nitrogen. Finally,
718 the extracted biofilm matrix was lyophilized using an ALPHA 1-4 LDplus freeze dryer (Christ, VWR) and
719 kept at -80 °C until sample preparation for proteomics.

720 The proteomics workflow included sample preparation, trypsin digestion, mass spectrometry, and
721 data analysis conducted as described in Herschend et al. [75] with some modifications.

722 **Matrix proteomics**

723 Freeze-dried samples were resuspended in 100 µL lysis buffer (6M Guanidinium Hydrochloride,
724 10mM TCEP, 40mM CAA, 50mM HEPES pH8.5) and sonicated for 2 minutes in a sonication bath
725 (Ultrasonic cleaner, VWR) at level 7-8. Samples were boiled for 5 min at 95 °C, spun down 10 min at
726 10000 rpm and 4 °C and supernatants transferred to Lo-bind microtiter plate. Protein content was quantified
727 with Pierce™ Rapid Gold BCA protein assay kit (Thermo Scientific) and 10 µg protein material was used
728 for digestion. The samples were three-fold diluted in digestion buffer (50 mM HEPES Ph 8.5 and 10%
729 acetonitrile) containing LysC (1:50 enzyme:protein ratio), briefly vortexed and incubated for 1 hour at 37
730 °C. Then samples were diluted 10x in digestion with trypsin (1:100 trypsin-to-protein ratio), briefly
731 vortexed and incubated at 37 °C temperature overnight. Inactivation of trypsin was achieved by adding
732 trifluoroacetic acid (TFA) to 2% and debris was removed by centrifugation (x g, 1 min 4 °C). Acidified
733 peptides were loaded onto a SOLAµ HRP 96-well plate for desalting, which was previously activated with
734 100% methanol, followed by 80% acetonitrile (AcN) complemented with 0.1% TFA and centrifugation at
735 1500 rpm for 1 min. SOLAµ HRP 96-well plate was then washed twice with 0.3% and 1% TFA and samples
736 loaded and washed twice using 200 µL 0.1% TFA before being eluted with 2 x 30 µl 40% AcN
737 complemented with 0.1% TFA. AcN was removed from eluted samples in a SpeedVac for at least 1 hour
738 and 60 °C. Dry peptide samples were resuspended in 12 µL A*iRT solution, sonicated for 60 seconds and
739 quantified using a DS-11 drop spectrophotometer. Desalted and purified peptide samples were kept at -80
740 °C until subjected to analysis by mass spectrometry.

741 **Mass Spectrometry analysis**

742 For each sample, peptides were loaded onto a 2cm C18 trap column (ThermoFisher 164705),
743 connected in-line to a 15cm C18 reverse-phase analytical column (Thermo EasySpray ES803) using 100%
744 Buffer A (0.1% Formic acid in water) at 750bar, using the Thermo EasyLC 1000 HPLC system, and the
745 column oven operating at 45 °C. Peptides were eluted over a 190 minute gradient ranging from 10 to 60%
746 of 80% acetonitrile, 0.1% formic acid at 250 nl/min, and the Q-Exactive instrument (Thermo Fisher
747 Scientific) was run in a DD-MS2 top10 method. Full MS spectra were collected at a resolution of 70,000
748 with an AGC target of 3×10^6 or maximum injection time of 20 ms and a scan range of 300–1750 m/z. The
749 MS2 spectra were obtained at a resolution of 17,500, with an AGC target value of 1×10^6 or maximum
750 injection time of 60 ms, a normalised collision energy of 25 and an intensity threshold of $1.7e^4$. Dynamic
751 exclusion was set to 60 s, and ions with a charge state <2 or unknown were excluded. MS performance was
752 verified for consistency by running complex cell lysate quality control standards, and chromatography was
753 monitored to check for reproducibility.

754 **Proteomics data analysis**

755 Peptides identified by mass spectrometry, representing a mixture from both species, were mapped
756 to the reference proteomes of *Bacillus thuringiensis* and *Pseudomonas brenneri* using MaxQuant
757 v1.6.10.43 [90] with the built-in Andromeda search engine [91]. A target decoy search that allowed for a
758 maximum of 1% FDR on both peptide and protein level and a minimum length of 7 amino acids per peptide
759 was performed. Quantification was performed using the label-free quantification (LFQ) algorithm [92] in
760 MaxQuant with a minimum ratio count of 2 and applying the "match between runs" function. The
761 Andromeda search engine was supplemented with the reference proteome of *Bacillus thuringiensis,* and/or
762 *Pseudomonas brenneri*. The genomes had been prepared during a previous study [29] and are available
763 online (NCBI) with the following IDs: IDs JARTVI000000000 (*B. thuringiensis*) and CP122540.1 (*P.*
764 *brenneri*).

765 Statistical analysis of proteomics data was performed with the Perseus software v1.6.15.0 [93] and
766 differentially expressed proteins were identified using a modified version of Welch's t-test with an S0
767 parameter of 0.5 [94] and a permutation-based FDR cut-off of 0.05 and valid values in at least 60% of the
768 samples in both sample groups, depending on the comparison made. In this software, pairwise comparisons
769 were performed for each species using the software Perseus: for *Bacillus thuringiensis*, monoculture versus
770 co-culture (for both ancestral and variant genotypes); and for *Pseudomonas brenneri*, monoculture versus
771 co-culture (including ancestral, V1, and V6 genotypes).

772 Prediction of subcellular localization of detected proteins was done using subcellular localization
773 prediction software PSORTb version 3.0.3 (https://www.psort.org/psortb/) [95]. Similarly, prediction
774 signal peptides and the location of their cleavage sites in the detected proteins was done using SignalP 6.0
775 (https://services.healthtech.dtu.dk/service.php?SignalP-6.0) [96].

776 **Statistical analysis and visualization**

777 All analyses and plotting were done in RStudio v4.1.1 [97] and package "ggplot2" v3.4.2. All datasets were
778 tested for normality and equal variance using the Shapiro-Wilk (base R) and Levene's (package "car"
779 v3.1.2) tests, respectively. Most datasets were not normally distributed and thereby a Kruskal-Wallis test
780 (base R) was used when comparing more than two groups, unless otherwise specified. A general expression
781 was kruskal.test(log10_CFUmL~Combination), however the quantitative variable and categorical variables
782 changed depending on the dataset. A Dunn´s post-hoc test was performed using package "FSA" v0.9.4 to
783 consider multiple comparisons when the Kruskal-Wallis test was significant, with a Bonferroni correction.
784 When comparing only two groups, a Wilcoxon´s rank test t-test was applied, usually comparing ancestor
785 and variant phenotype/genotype (i.e. wilcox.test (CFU~Phenotype)). A *p*-value of 0.05 was used as a
786 threshold for statistical significance ($p < 0.05$). Compact letter display for multiple comparisons was
787 calculated using the R package "rcompanion" v2.4.35.

Competing interests

The authors declare no competing interests.

Acknowledgments

The authors thank Sara Olsen and Anette Løth for technical assistance, the DTU Proteomics core facility for technical assistance in proteomics sample preparation. Support by Ute Kuhlicke with lectin analysis and confocal laser scanning microscopy is highly appreciated. We thank the Villum Foundation for grants to MB (no. 10098) and HR (no. 34434) and the US Office of Naval Research, for grant N629091812174 to MB, as well as the Swiss National Science Foundation Consolidator Grant TMCG-3_213801 to KD, and the German Bundesministerium für Bildung und Forschung grant TARGET-Biofilms 16GW0245 to KD, funding this work.

Data availability statement

B. thuringiensis and *P. brenneri* genomes are available online at NCBI (https://www.ncbi.nlm.nih.gov/genome/) with the following IDs: JARTVI000000000 and CP122540.1, respectively. The mass spectrometry proteomics raw data and results from analysis by MaxQuant have been deposited to the ProteomeXchange Consortium via the PRIDE [98] partner repository with the dataset identifier PXD046156 (https://www.ebi.ac.uk/pride/archive). The data is currently private and can only be accessed with a single reviewer account that has been created. The data will be publicly available when accepted for publication. For reviewer access, use the username reviewer_pxd046156@ebi.ac.uk and password kkAMO14X.

807 # References

808 1. Agrawal AA. Phenotypic plasticity in the interactions and evolution of species. *Science* 2001; **294**:
809 321–326.
810 2. Barrett RDH, Schluter D. Adaptation from standing genetic variation. *Trends Ecol Evol* 2008; **23**: 38–
811 44.
812 3. Barrick JE, Lenski RE. Genome dynamics during experimental evolution. *Nat Rev Genet 2013 1412*
813 2013; **14**: 827–839.
814 4. Scheuerl T, Hopkins M, Nowell RW, Rivett DW, Barraclough TG, Bell T. Bacterial adaptation is
815 constrained in complex communities. *Nat Commun* 2020; **11**: 1–8.
816 5. Calcagno V, Jarne P, Loreau M, Mouquet N, David P. Diversity spurs diversification in ecological
817 communities. *Nat Commun* 2017; **8**.
818 6. Emerson BC, Kolm N. Species diversity can drive speciation. *Nature* 2005; **434**: 1015–1017.
819 7. Nadell CD, Xavier JB, Foster KR. The sociobiology of biofilms. *FEMS Microbiol Rev* 2009; **33**: 206–
820 224.
821 8. Gross K, Cardinale BJ. Does species richness drive community production or vice versa? Reconciling
822 historical and contemporary paradigms in competitive communities. *Am Nat* 2007; **170**: 207–220.
823 9. Cardinale BJ, Wright JP, Cadotte MW, Carroll IT, Hector A, Srivastava DS, et al. Impacts of plant
824 diversity on biomass production increase through time because of species complementarity. *Proc Natl*
825 *Acad Sci U S A* 2007; **104**: 18123–18128.
826 10. Nadell CD, Drescher K, Foster KR. Spatial structure, cooperation and competition in biofilms. *Nat*
827 *Rev Microbiol 2016 149* 2016; **14**: 589–600.
828 11. Rainey PB, Travisano M. Adaptive radiation in a heterogeneous environment. *Nature* 1998; **394**: 69–
829 72.
830 12. Habets MGJL, Rozen DE, Hoekstra RF, De Visser JAGM. The effect of population structure on the
831 adaptive radiation of microbial populations evolving in spatially structured environments. *Ecol Lett*
832 2006; **9**: 1041–1048.
833 13. Foster KR, Bell T. Competition, not cooperation, dominates interactions among culturable microbial
834 species. *Curr Biol* 2012; **22**: 1845–1850.
835 14. Xavier JB, Foster KR. Cooperation and conflict in microbial biofilms. *Proc Natl Acad Sci U S A*
836 2007; **104**: 876–881.
837 15. Rao D, Webb JS, Kjelleberg S. Competitive interactions in mixed-species biofilms containing the
838 marine bacterium Pseudoalteromonas tunicata. *Appl Environ Microbiol* 2005; **71**: 1729–1736.
839 16. Hibbing ME, Fuqua C, Parsek MR, Peterson SB. Bacterial competition: surviving and thriving in the

840 microbial jungle. *Nat Rev Microbiol* 2010; **8**: 15.
841 17. Ghoul M, Mitri S. The Ecology and Evolution of Microbial Competition. *Trends Microbiol* 2016; **24**:
842 833–845.
843 18. Røder HL, Herschend J, Russel J, Andersen MF, Madsen JS, Sørensen SJ, et al. Enhanced bacterial
844 mutualism through an evolved biofilm phenotype. *ISME J* 2018; **12**: 2608.
845 19. Liu W, Jacquiod S, Brejnrod A, Russel J, Burmølle M, Sørensen SJ. Deciphering links between
846 bacterial interactions and spatial organization in multispecies biofilms. *ISME J* 2019; **13**: 3054–3066.
847 20. Henriksen NNSE, Hansen MF, Kiesewalter HT, Russel J, Nesme J, Foster KR, et al. Biofilm
848 cultivation facilitates coexistence and adaptive evolution in an industrial bacterial community. *NPJ*
849 *biofilms microbiomes* 2022; **8**.
850 21. McDonald MJ, Gehrig SM, Meintjes PL, Zhang XX, Rainey PB. Adaptive Divergence in
851 Experimental Populations of Pseudomonas fluorescens. IV. Genetic Constraints Guide Evolutionary
852 Trajectories in a Parallel Adaptive Radiation. *Genetics* 2009; **183**: 1041.
853 22. Traverse CC, Mayo-Smith LM, Poltak SR, Cooper VS. Tangled bank of experimentally evolved
854 Burkholderia biofilms reflects selection during chronic infections. *Proc Natl Acad Sci U S A* 2013;
855 **110**: E250–E259.
856 23. Thöming JG, Tomasch J, Preusse M, Koska M, Grahl N, Pohl S, et al. Parallel evolutionary paths to
857 produce more than one Pseudomonas aeruginosa biofilm phenotype. *NPJ Biofilms Microbiomes* 2020;
858 **6**.
859 24. Leiman SA, Arboleda LC, Spina JS, McLoon AL. SinR is a mutational target for fine-tuning biofilm
860 formation in laboratory-evolved strains of Bacillus subtilis. *BMC Microbiol* 2014; **14**.
861 25. Dragoš A, Lakshmanan N, Martin M, Horváth B, Maróti G, García CF, et al. Evolution of exploitative
862 interactions during diversification in Bacillus subtilis biofilms. *FEMS Microbiol Ecol* 2018; **94**.
863 26. Lin Y, Xu X, Maróti G, Strube ML, Kovács ÁT. Adaptation and phenotypic diversification of
864 Bacillus thuringiensis biofilm are accompanied by fuzzy spreader morphotypes. *npj Biofilms*
865 *Microbiomes 2022 81* 2022; **8**: 1–14.
866 27. Pomerleau M, Charron-Lamoureux V, Léonard L, Grenier F, Rodrigue S, Beauregard PB. Adaptive
867 laboratory evolution reveals regulators involved in repressing biofilm development as key players in
868 Bacillus subtilis root colonization. *mSystems* 2024; **9:e00843**.
869 28. Ehling-Schulz M, Koehler TM, Lereclus D. The Bacillus cereus Group: Bacillus species with
870 Pathogenic Potential. *Microbiol Spectr* 2019; **7**.
871 29. Maccario L, Silva AF, Nesme J, Amador CI, Sørensen SJ, Cooper VS, et al. Draft genomes of seven
872 isolates from Danish wastewater facilities belonging to Pseudomonas , Bacillus , Pseudochrobactrum ,
873 Brevundimonas , and Pandoraea . *Microbiol Resour Announc* 2023; **12**.

874 30. Muthukumar A, Raj TS, Prabhukarthikeyan SR, Naveen R, Keerthanab U. Pseudomonas and
875 Bacillus: A biological tool for crop protection. *New and Future Developments in Microbial*
876 *Biotechnology and Bioengineering: Sustainable Agriculture: Advances in Microbe-based*
877 *Biostimulants*. 2022. Elsevier, pp 145–158.
878 31. Lyng M, Kovács ÁT. Frenemies of the soil: Bacillus and Pseudomonas interspecies interactions.
879 *Trends Microbiol* 2023; **31**: 845–857.
880 32. Poltak SR, Cooper VS. Ecological succession in long-term experimentally evolved biofilms produces
881 synergistic communities. *ISME J* 2011; **5**: 369.
882 33. Koh KS, Lam KW, Alhede M, Queck SY, Labbate M, Kjelleberg S, et al. Phenotypic Diversification
883 and Adaptation of Serratia marcescens MG1 Biofilm-Derived Morphotypes. *J Bacteriol* 2006; **189**:
884 119.
885 34. Johns BE, Purdy KJ, Tucker NP, Maddocks SE. Phenotypic and Genotypic Characteristics of Small
886 Colony Variants and Their Role in Chronic Infection. *Microbiol Insights* 2015; **8**: 15.
887 35. Zhou Y, Blanco LP, Smith DR, Chapman MR. Bacterial Amyloids. *Methods Mol Biol* 2012; **849**:
888 303.
889 36. Jones CJ, Wozniak DJ. Congo red stain identifies matrix overproduction and is an indirect
890 measurement for c-di-GMP in many species of bacteria. *Methods Mol Biol* 2017; **1657**: 147–156.
891 37. Trunk T, Khalil HS, Leo JC. Bacterial autoaggregation. *AIMS Microbiol* 2018; **4**: 140.
892 38. Amador CI, Canosa I, Govantes F, Santero E. Lack of CbrB in Pseudomonas putida affects not only
893 amino acids metabolism but also different stress responses and biofilm development. *Environ*
894 *Microbiol* 2010; **12**: 1748–1761.
895 39. Lopes Da Silva T, Reis A, Kent CA, Roseiro JC, Hewitt CJ. The use of multi-parameter flow
896 cytometry to study the impact of limiting substrate, agitation intensity, and dilution rate on cell
897 aggregation during Bacillus licheniformis CCMI 1034 aerobic continuous culture fermentations.
898 *Biotechnol Bioeng* 2005; **92**: 568–578.
899 40. Ojima Y, Matano S, Azuma M. Characterization of self-aggregation in Bacillus licheniformis strain
900 RK14. *Ann Microbiol* 2023; **73**: 1–7.
901 41. Fawcett P, Eichenberger P, Losick R, Youngman P. The transcriptional profile of early to middle
902 sporulation in Bacillus subtilis. *Proc Natl Acad Sci U S A* 2000; **97**: 8063–8068.
903 42. Molle V, Fujita M, Jensen ST, Eichenberger P, González-Pastor JE, Liu JS, et al. The Spo0A regulon
904 of Bacillus subtilis. *Mol Microbiol* 2003; **50**: 1683–1701.
905 43. Deatherage DE, Traverse CC, Wolf LN, Barrick JE. Detecting rare structural variation in evolving
906 microbial populations from new sequence junctions using breseq. *Front Genet* 2015; **5**.
907 44. Roberts DM. A new role for monomeric ParA/Soj in chromosome dynamics in Bacillus subtilis.

908 *Microbiologyopen* 2023; **12**: e1344.
909 45. Neu TR, Kuhlicke U. Matrix glycoconjugate characterization in multispecies biofilms and
910 bioaggregates from the environment by means of fluorescently-labeled lectins. *Front Microbiol* 2022;
911 **13**.
912 46. Vollmer W, Blanot D, De Pedro MA. Peptidoglycan structure and architecture. *FEMS Microbiol Rev*
913 2008; **32**: 149–167.
914 47. Tännler S, Decasper S, Sauer U. Maintenance metabolism and carbon fluxes in Bacillus species.
915 *Microb Cell Fact* 2008; **7**: 19.
916 48. Fischer E, Sauer U. Large-scale in vivo flux analysis shows rigidity and suboptimal performance of
917 Bacillus subtilis metabolism. *Nat Genet 2005 376* 2005; **37**: 636–640.
918 49. Hansen SK, Rainey PB, Haagensen JAJ, Molin S. Evolution of species interactions in a biofilm
919 community. *Nature* 2007; **445**: 533–536.
920 50. Cosetta CM, Niccum B, Kamkari N, Dente M, Podniesinski M, Wolfe BE. Bacterial–fungal
921 interactions promote parallel evolution of global transcriptional regulators in a widespread
922 Staphylococcus species. *ISME J 2023 179* 2023; **17**: 1504–1516.
923 51. Vishnoi M, Narula J, Devi SN, Dao HA, Igoshin OA, Fujita M. Triggering sporulation in Bacillus
924 subtilis with artificial two-component systems reveals the importance of proper Spo0A activation
925 dynamics. *Mol Microbiol* 2013; **90**: 181–194.
926 52. Huang Y, Flint SH, Palmer JS. Bacillus cereus spores and toxins – The potential role of biofilms.
927 *Food Microbiol* 2020; **90**: 103493.
928 53. Hamon MA, Lazazzera BA. The sporulation transcription factor Spo0A is required for biofilm
929 development in Bacillus subtilis. *Mol Microbiol* 2001; **42**: 1199–1209.
930 54. Xu S, Yang N, Zheng S, Yan F, Jiang C, Yu Y, et al. The spo0A-sinI-sinR Regulatory Circuit Plays
931 an Essential Role in Biofilm Formation, Nematicidal Activities, and Plant Protection in Bacillus cereus
932 AR156. *Mol Plant Microbe Interact* 2017; **30**: 603–619.
933 55. Huang R, Shao J, Xu Z, Chen Y, Liu Y, Wang D, et al. A toxin-mediated policing system in Bacillus
934 optimizes division of labor via penalizing cheater-like nonproducers. *Elife* 2023; **12**: 84743.
935 56. Sharipova M, Rudakova N, Mardanova A, Evtugyn V, Akosah Y, Danilova I, et al. Biofilm
936 Formation by Mutant Strains of Bacilli under Different Stress Conditions. *Microorganisms* 2023;
937 **11(6)**, **148**.
938 57. Periwal V, Scaria V. Insights into structural variations and genome rearrangements in prokaryotic
939 genomes. *Bioinformatics* 2015; **31**: 1–9.
940 58. Raeside C, Gaffé J, Deatherage DE, Tenaillon O, Briska AM, Ptashkin RN, et al. Large chromosomal
941 rearrangements during a long-term evolution experiment with Escherichia coli. *MBio* 2014; **5**: 1377–

942 1391.
943 59. Nishikawa M, Kobayashi K. Calcium Prevents Biofilm Dispersion in Bacillus subtilis. *J Bacteriol*
944 2021; **203**.
945 60. Rousset L, Alpha-Bazin B, Château A, Armengaud J, Clavel T, Berge O, et al. Groundwater promotes
946 emergence of asporogenic mutants of emetic Bacillus cereus. *Environ Microbiol* 2020; **22**: 5248–
947 5264.
948 61. Antequera-Gómez ML, Díaz-Martínez L, Guadix JA, Sánchez-Tévar AM, Sopeña-Torres S,
949 Hierrezuelo J, et al. Sporulation is dispensable for the vegetable-associated life cycle of the human
950 pathogen Bacillus cereus. *Microb Biotechnol* 2021; **14**: 1550–1565.
951 62. Dubois T, Faegri K, Gélis-Jeanvoine S, Perchat S, Lemy C, Buisson C, et al. Correction:
952 Necrotrophism Is a Quorum-Sensing-Regulated Lifestyle in Bacillus thuringiensis. *PLoS Pathog* 2016;
953 **12**.
954 63. Romero D, Aguilar C, Losick R, Kolter R. Amyloid fibers provide structural integrity to Bacillus
955 subtilis biofilms. *Proc Natl Acad Sci U S A* 2010; **107**: 2230–2234.
956 64. Branda SS, Chu F, Kearns DB, Losick R, Kolter R. A major protein component of the Bacillus
957 subtilis biofilm matrix. *Mol Microbiol* 2006; **59**: 1229–1238.
958 65. Lakshmanan V, Kitto SL, Caplan JL, Hsueh Y-H, Kearns DB, Wu Y-S, et al. Microbe-Associated
959 Molecular Patterns-Triggered Root Responses Mediate Beneficial Rhizobacterial Recruitment in
960 Arabidopsis 1[C][W][OA]. *Plant Physiol Ò* 2003; **160**: 1642–1661.
961 66. Candela T, Fagerlund A, Buisson C, Gilois N, Kolstø AB, Økstad OA, et al. CalY is a major virulence
962 factor and a biofilm matrix protein. *Mol Microbiol* 2019; **111**: 1416–1429.
963 67. Chen M, Lyu Y, Feng E, Zhu L, Pan C, Wang D, et al. SpoVG Is Necessary for Sporulation in
964 Bacillus anthracis. *Microorganisms* 2020; **8(4)**, **548**.
965 68. Huang Q, Zhang Z, Liu Q, Liu F, Liu Y, Zhang J, et al. SpoVG is an important regulator of
966 sporulation and affects biofilm formation by regulating Spo0A transcription in Bacillus cereus 0–9.
967 *BMC Microbiol* 2021; **21**: 1–17.
968 69. Lin Y, Briandet R, Kovács ÁT. Bacillus cereus sensu lato biofilm formation and its ecological
969 importance. *Biofilm* . 2022. , **4**, **100070**
970 70. Livingston ET, Mursalin MH, Coburn PS, Astley R, Miller FC, Amayem O, et al. Immune inhibitor a
971 metalloproteases contribute to virulence in Bacillus endophthalmitis. *Infect Immun* 2021; **89**.
972 71. Harwood CR, Kikuchi Y. The ins and outs of Bacillus proteases: activities, functions and commercial
973 significance. *FEMS Microbiol Rev* 2022; **46**: 1–20.
974 72. Grandvalet C, Gominet M, Lereclus D. Identification of genes involved in the activation of the
975 Bacillus thuringiensis inhA metalloprotease gene at the onset of sporulation. *Microbiology* 2001; **147**:

976 1805–1813.
977 73. Pflughoeft KJ, Sumby P, Koehler TM. Bacillus anthracis sin locus and regulation of secreted
978 proteases. *J Bacteriol* 2011; **193**: 631–639.
979 74. Hansen LBS, Ren D, Burmølle M, Sørensen SJ. Distinct gene expression profile of Xanthomonas
980 retroflexus engaged in synergistic multispecies biofilm formation. *ISME J* 2017; **11**: 300–303.
981 75. Herschend J, Damholt ZBV, Marquard AM, Svensson B, Sørensen SJ, Hägglund P, et al. A meta-
982 proteomics approach to study the interspecies interactions affecting microbial biofilm development in
983 a model community. *Sci Rep* 2017; **7**: 16483.
984 76. Ratzke C, Gore J. Modifying and reacting to the environmental pH can drive bacterial interactions.
985 *PLoS Biol* 2018; **16(3)**: e2004248.
986 77. Herschend J, Koren K, Røder HL, Brejnrod A, Kühl M, Burmølle M. In Vitro Community Synergy
987 between Bacterial Soil Isolates Can Be Facilitated by pH Stabilization of the Environment. *Appl*
988 *Environ Microbiol* 2018; **84**: e01450-18.
989 78. Pacheco AR, Segrè D. A multidimensional perspective on microbial interactions. *FEMS Microbiol*
990 *Lett* 2019; **366**: 125.
991 79. Aranda-Díaz A, Obadia B, Dodge R, Thomsen T, Hallberg ZF, Güvener ZT, et al. Bacterial
992 interspecies interactions modulate pH-mediated antibiotic tolerance. *Elife* 2020; **9**.
993 80. Fritts RK, McCully AL, McKinlay JB. Extracellular Metabolism Sets the Table for Microbial Cross-
994 Feeding. *Microbiol Mol Biol Rev* 2021; **85**.
995 81. O'Toole G, Kolter R. Initiation of biofilm formation in Pseudomonas fluorescens WCS365 proceeds
996 via multiple, convergent signalling pathways: a genetic analysis. *Mol Microbiol* 1998; **28**: 449–461.
997 82. Sprouffske K, Wagner A. Growthcurver: An R package for obtaining interpretable metrics from
998 microbial growth curves. *BMC Bioinformatics* 2016; **17**: 1–4.
999 83. Deatherage DE, Barrick JE. Identification of mutations in laboratory-evolved microbes from next-
1000 generation sequencing data using breseq. *Methods Mol Biol* 2014; **1151**: 165–188.
1001 84. Toukabri H, Lereclus D, Slamti L. A Sporulation-Independent Way of Life for Bacillus thuringiensis
1002 in the Late Stages of an Infection. *MBio* 2023; **14**.
1003 85. Neu T, Kuhlicke U. Fluorescence Lectin Bar-Coding of Glycoconjugates in the Extracellular Matrix
1004 of Biofilm and Bioaggregate Forming Microorganisms. *Microorganisms* 2017.
1005 86. Hartmann R, Jeckel H, Jelli E, Singh PK, Vaidya S, Bayer M, et al. Quantitative image analysis of
1006 microbial communities with BiofilmQ. *Nat Microbiol 2021 62* 2021; **6**: 151–156.
1007 87. Liu H, Fang HHP. Extraction of extracellular polymeric substances (EPS) of sludges. *J Biotechnol*
1008 2002; **95**: 249–256.
1009 88. Pan X, Liu J, Zhang D, Chen XI, Li L, Song W, et al. A comparison of five extraction methods for

1010 extracellular polymeric substances (EPS) from biofilm by using three-dimensional excitation-emission
1011 matrix (3DEEM) fluorescence spectroscopy. *undefined* 2010; **36**: 111–116.
1012 89. Bradford MM. A rapid and sensitive method for the quantitation of microgram quantities of protein
1013 utilizing the principle of protein-dye binding. *Anal Biochem* 1976; **72**: 248–254.
1014 90. Cox J, Mann M. MaxQuant enables high peptide identification rates, individualized p.p.b.-range mass
1015 accuracies and proteome-wide protein quantification. *Nat Biotechnol* 2008; **26**: 1367–1372.
1016 91. Cox J, Neuhauser N, Michalski A, Scheltema RA, Olsen J V., Mann M. Andromeda: a peptide search
1017 engine integrated into the MaxQuant environment. *J Proteome Res* 2011; **10**: 1794–1805.
1018 92. Cox J, Hein MY, Luber CA, Paron I, Nagaraj N, Mann M. Accurate Proteome-wide Label-free
1019 Quantification by Delayed Normalization and Maximal Peptide Ratio Extraction, Termed MaxLFQ.
1020 *Mol Cell Proteomics* 2014; **13**: 2513.
1021 93. Tyanova S, Temu T, Sinitcyn P, Carlson A, Hein MY, Geiger T, et al. The Perseus computational
1022 platform for comprehensive analysis of (prote)omics data. *Nat Methods 2016 139* 2016; **13**: 731–740.
1023 94. Tusher VG, Tibshirani R, Chu G. Significance analysis of microarrays applied to the ionizing
1024 radiation response. *Proc Natl Acad Sci U S A* 2001; **98**: 5116–5121.
1025 95. Yu NY, Wagner JR, Laird MR, Melli G, Rey S, Lo R, et al. PSORTb 3.0: improved protein
1026 subcellular localization prediction with refined localization subcategories and predictive capabilities
1027 for all prokaryotes. *Bioinformatics* 2010; **26**: 1608–1615.
1028 96. Teufel F, Almagro Armenteros JJ, Johansen AR, Gíslason MH, Pihl SI, Tsirigos KD, et al. SignalP
1029 6.0 predicts all five types of signal peptides using protein language models. *Nat Biotechnol 2022 407*
1030 2022; **40**: 1023–1025.
1031 97. Team. RStudio: Integrated Development for R. *Rstudio, BMC* 2021.
1032 98. Perez-Riverol Y, Bai J, Bandla C, García-Seisdedos D, Hewapathirana S, Kamatchinathan S, et al.
1033 The PRIDE database resources in 2022: a hub for mass spectrometry-based proteomics evidences.
1034 *Nucleic Acids Res* 2022; **50**: D543–D552.
1035 99. Grandvalet C, Gominet M, Lereclus D. Identification of genes involved in the activation of the
1036 Bacillus thuringiensis inhA metalloprotease gene at the onset of sporulation. *Microbiology* 2001; **147**:
1037 1805–1813.
1038

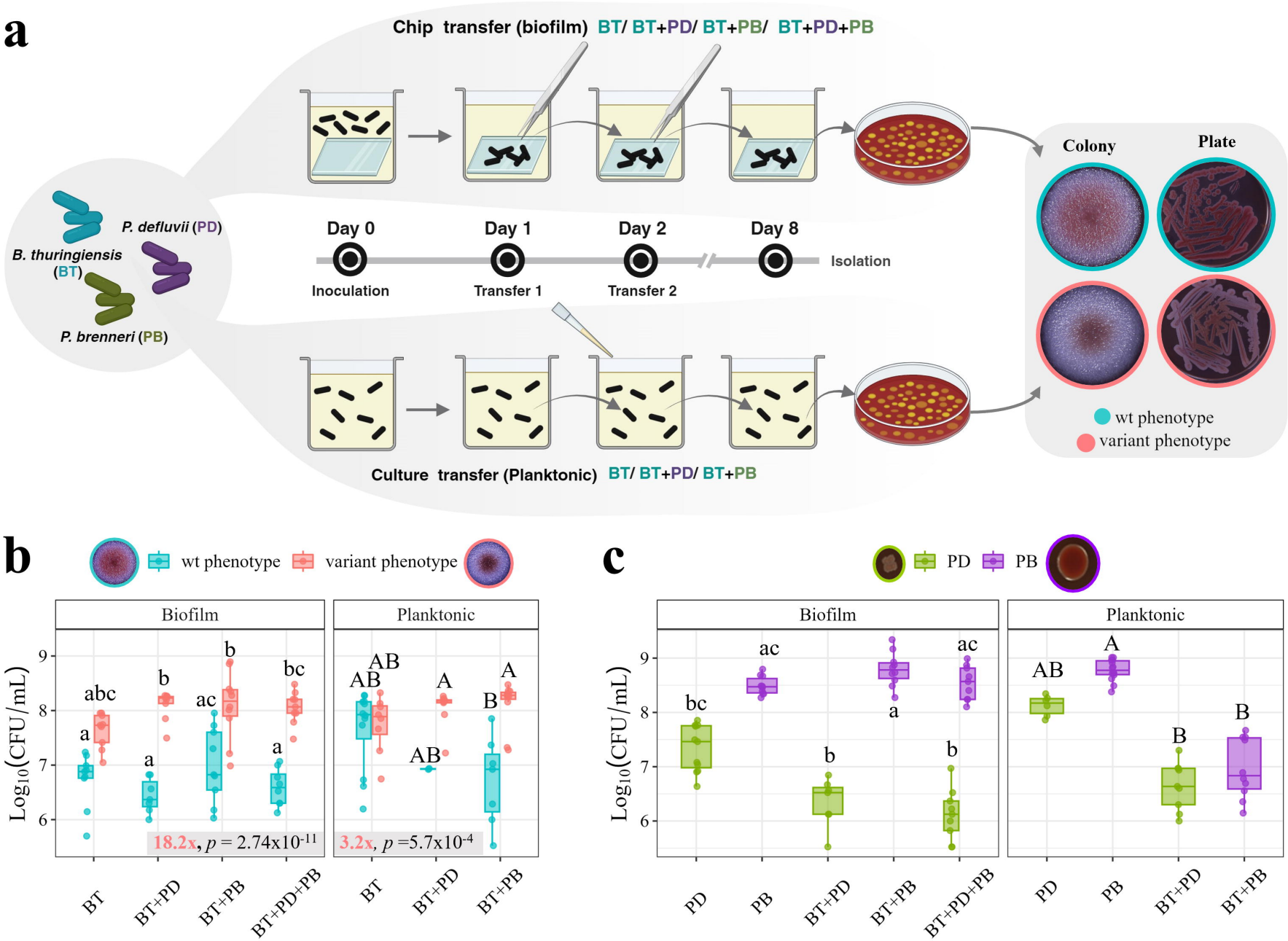
a
Chip transfer (biofilm) BT/ BT+PD/ BT+PB/ BT+PD+PB
P. defluvii (PD)
B. thuringiensis (BT)
P. brenneri (PB)
Day 0
Day 1
Day 2
Day 8
Isolation
Inoculation
Transfer 1
Transfer 2
Colony
Plate
wt phenotype
variant phenotype
Culture transfer (Planktonic) BT/ BT+PD/ BT+PB
b
wt phenotype
variant phenotype
Biofilm
Planktonic
Log10(CFU/mL)
18.2x, p = 2.74x10-11
3.2x, p =5.7x10-4
BT
BT+PD
BT+PB
BT+PD+PB
c
PD
PB
Biofilm
Planktonic
Log10(CFU/mL)
PD
PB
BT+PD
BT+PB
BT+PD+PB

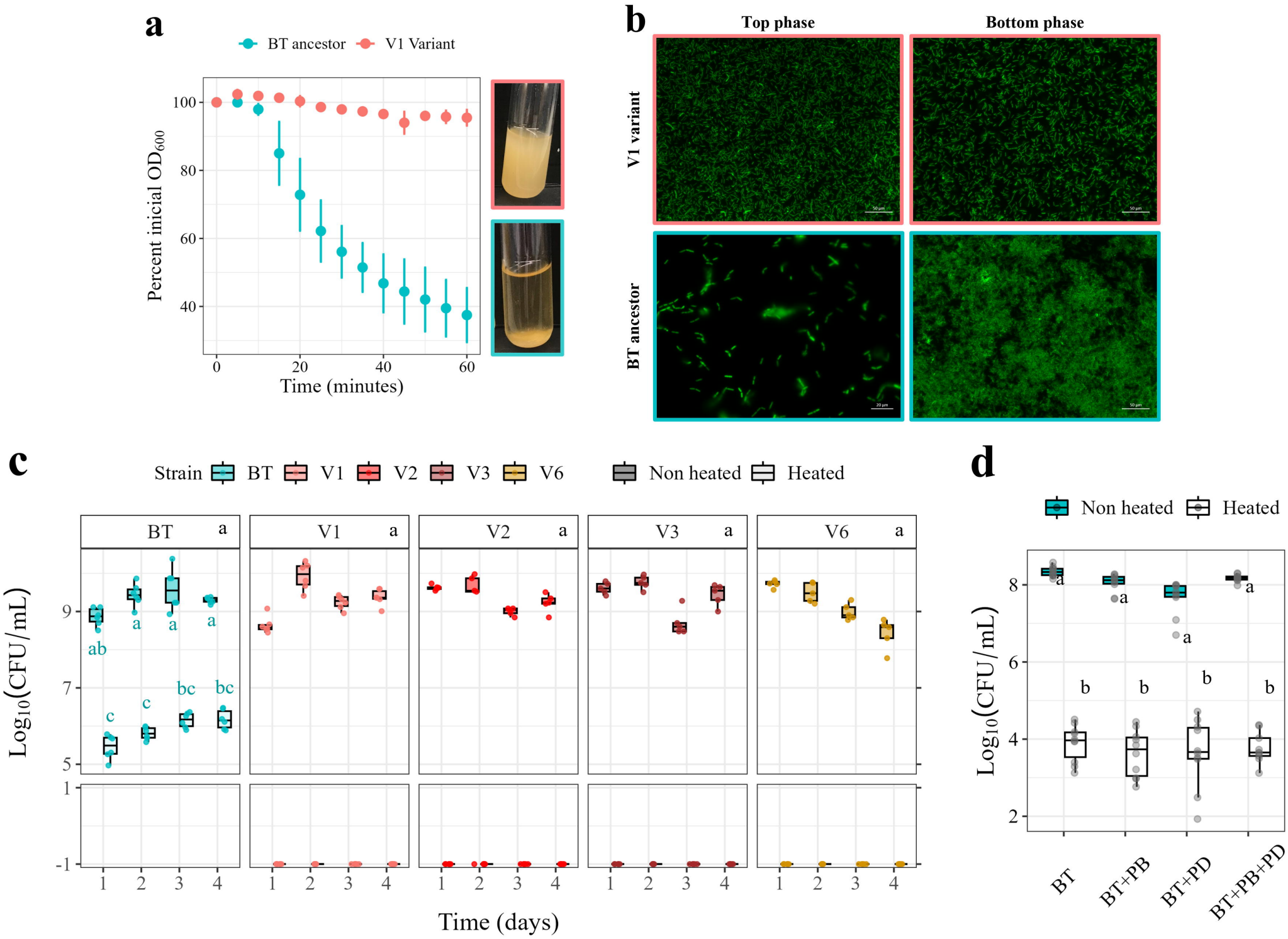
a
BT ancestor
V1 Variant
Percent inicial OD600
Time (minutes)
b
Top phase
Bottom phase
V1 variant
BT ancestor
c
Strain
BT
V1
V2
V3
V6
Non heated
Heated
Log10(CFU/mL)
Time (days)
d
Non heated
Heated
Log10(CFU/mL)
BT
BT+PB
BT+PD
BT+PB+PD

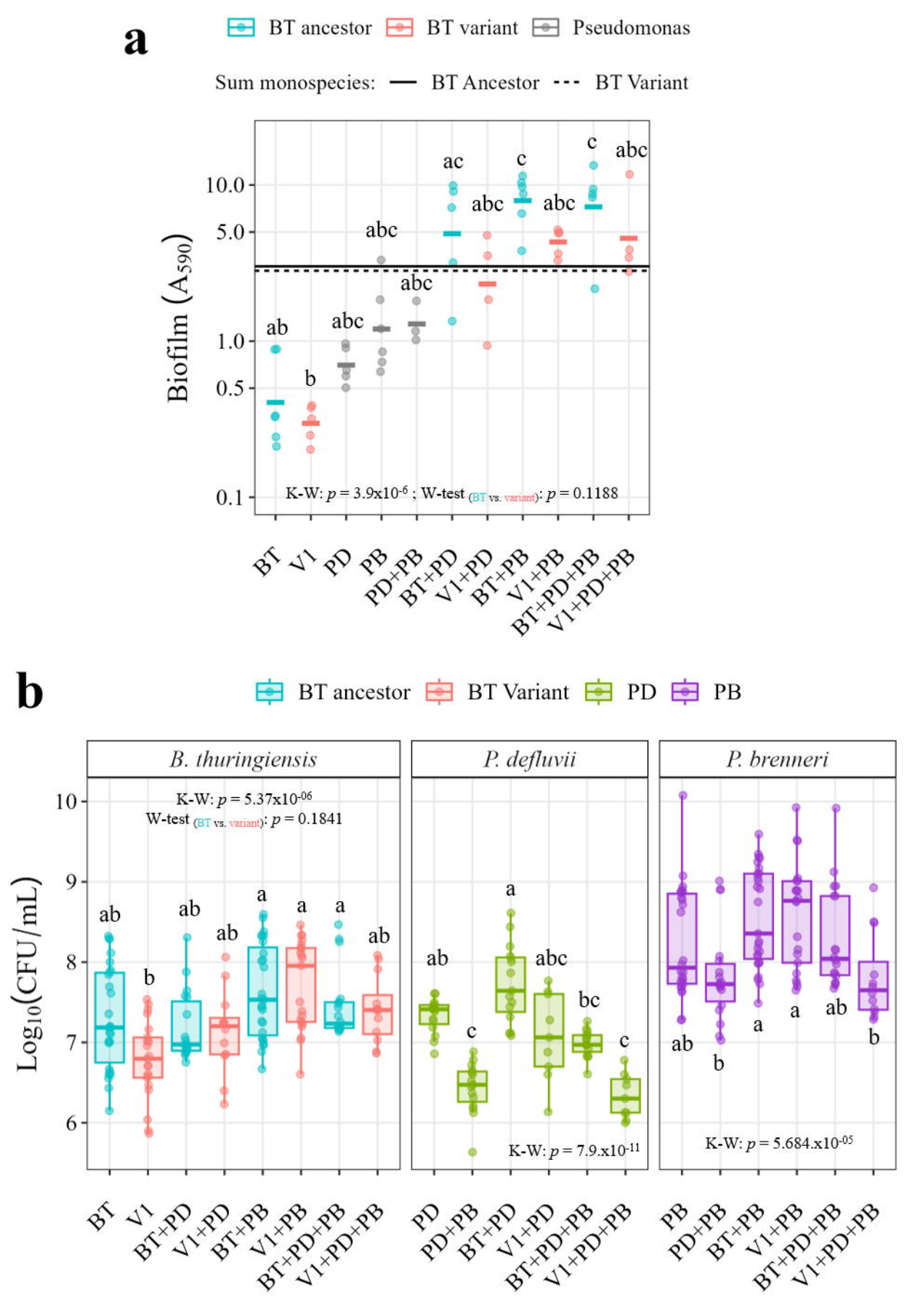
a
BT ancestor
BT variant
Pseudomonas
Sum monospecies:
BT Ancestor
BT Variant
Biofilm (A_{590})
10.0
5.0
1.0
0.5
0.1
ab
b
abc
abc
abc
ac
abc
c
abc
c
abc
K-W: $p = 3.9x10^{-6}$; W-test (BT vs. variant): $p = 0.1188$
BT
V1
PD
PB
PD+PB
BT+PD
V1+PD
BT+PB
V1+PB
BT+PD+PB
V1+PD+PB
b
BT ancestor
BT Variant
PD
PB
B. thuringiensis
P. defluvii
P. brenneri
Log10(CFU/mL)
10
9
8
7
6
K-W: $p = 5.37x10^{-06}$
W-test (BT vs. variant): $p = 0.1841$
ab
b
ab
ab
a
a
a
ab
ab
c
a
abc
bc
c
K-W: $p = 7.9.x10^{-11}$
ab
b
a
a
ab
b
K-W: $p = 5.684.x10^{-05}$
BT
V1
BT+PD
V1+PD
BT+PB
V1+PB
BT+PD+PB
V1+PD+PB
PD
PD+PB
BT+PD
V1+PD
BT+PD+PB
V1+PD+PB
PB
PD+PB
BT+PB
V1+PB
BT+PD+PB
V1+PD+PB

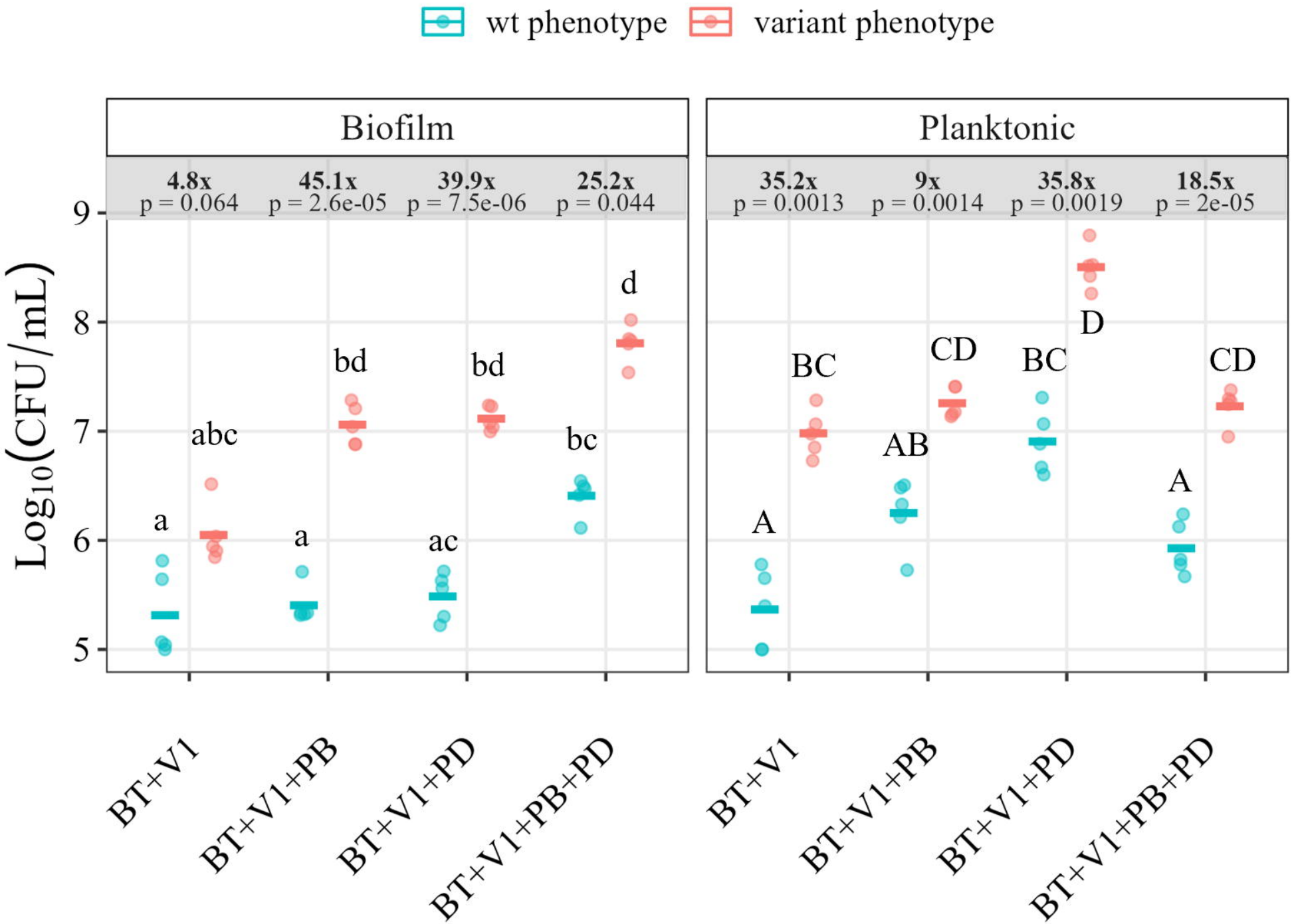
wt phenotype
variant phenotype
Biofilm
Planktonic
4.8x
p = 0.064
45.1x
p = 2.6e-05
39.9x
p = 7.5e-06
25.2x
p = 0.044
35.2x
p = 0.0013
9x
p = 0.0014
35.8x
p = 0.0019
18.5x
p = 2e-05
Log10(CFU/mL)
9
8
7
6
5
a
abc
a
ac
bd
bd
bc
d
A
BC
AB
CD
BC
D
A
CD
BT+V1
BT+V1+PB
BT+V1+PD
BT+V1+PB+PD

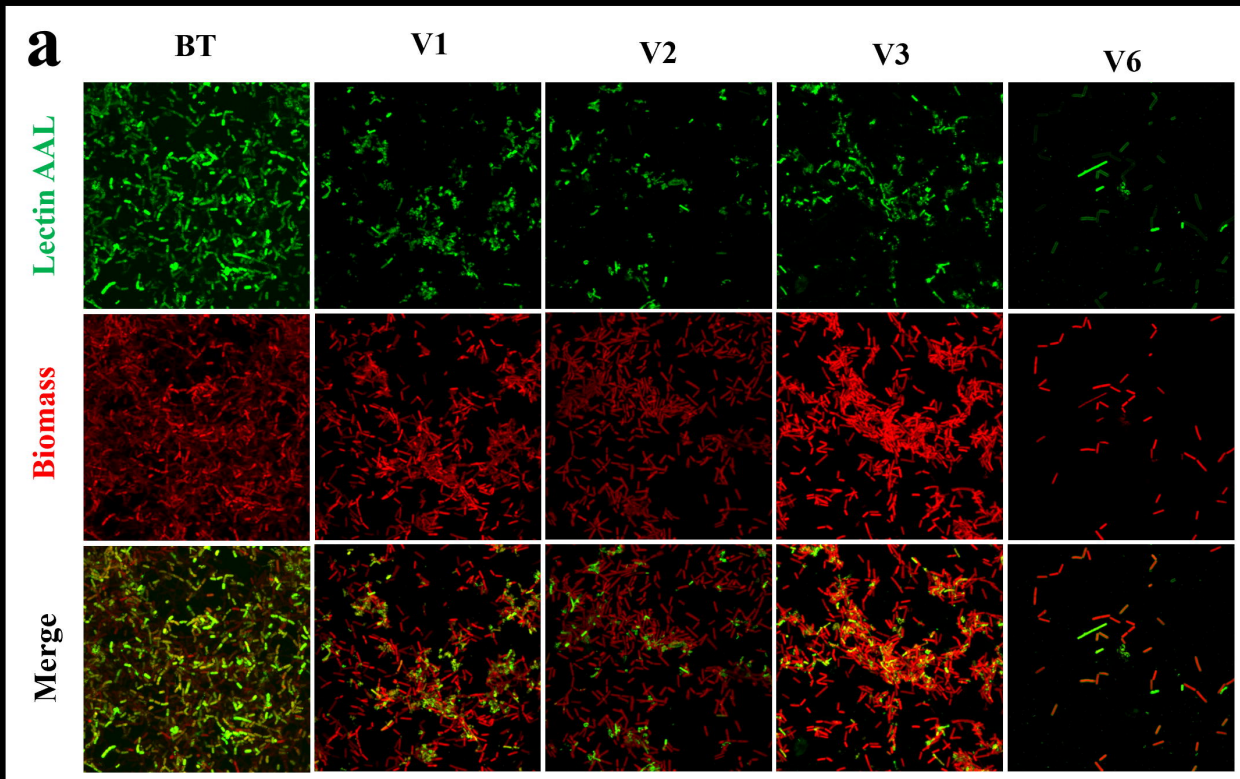
a
BT
V1
V2
V3
V6
Lectin AAL
Biomass
Merge

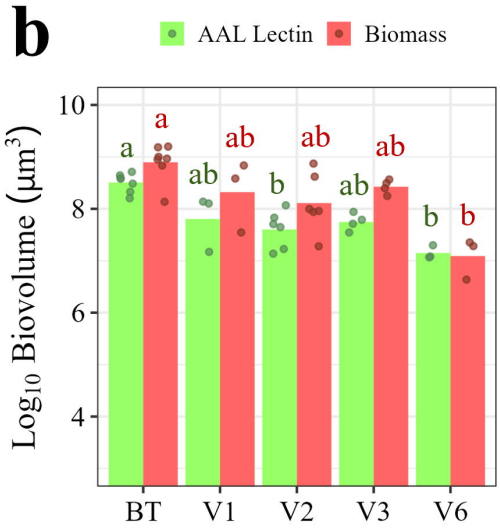
b
AAL Lectin
Biomass
Log10 Biovolume (µm3)
10
8
6
4
a
a
ab
ab
b
ab
ab
ab
b
b
BT
V1
V2
V3
V6

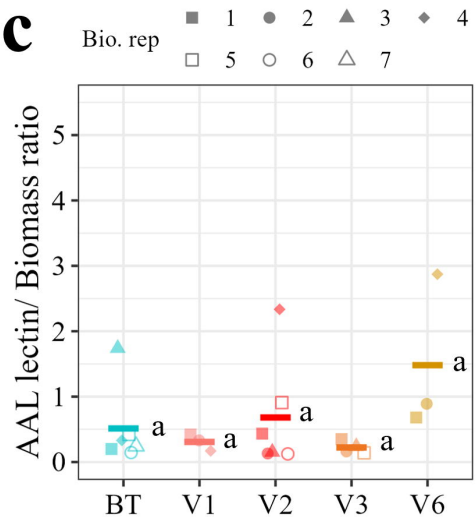
c
Bio. rep
1
2
3
4
5
6
7
AAL lectin/ Biomass ratio
5
4
3
2
1
0
a
a
a
a
a
BT
V1
V2
V3
V6

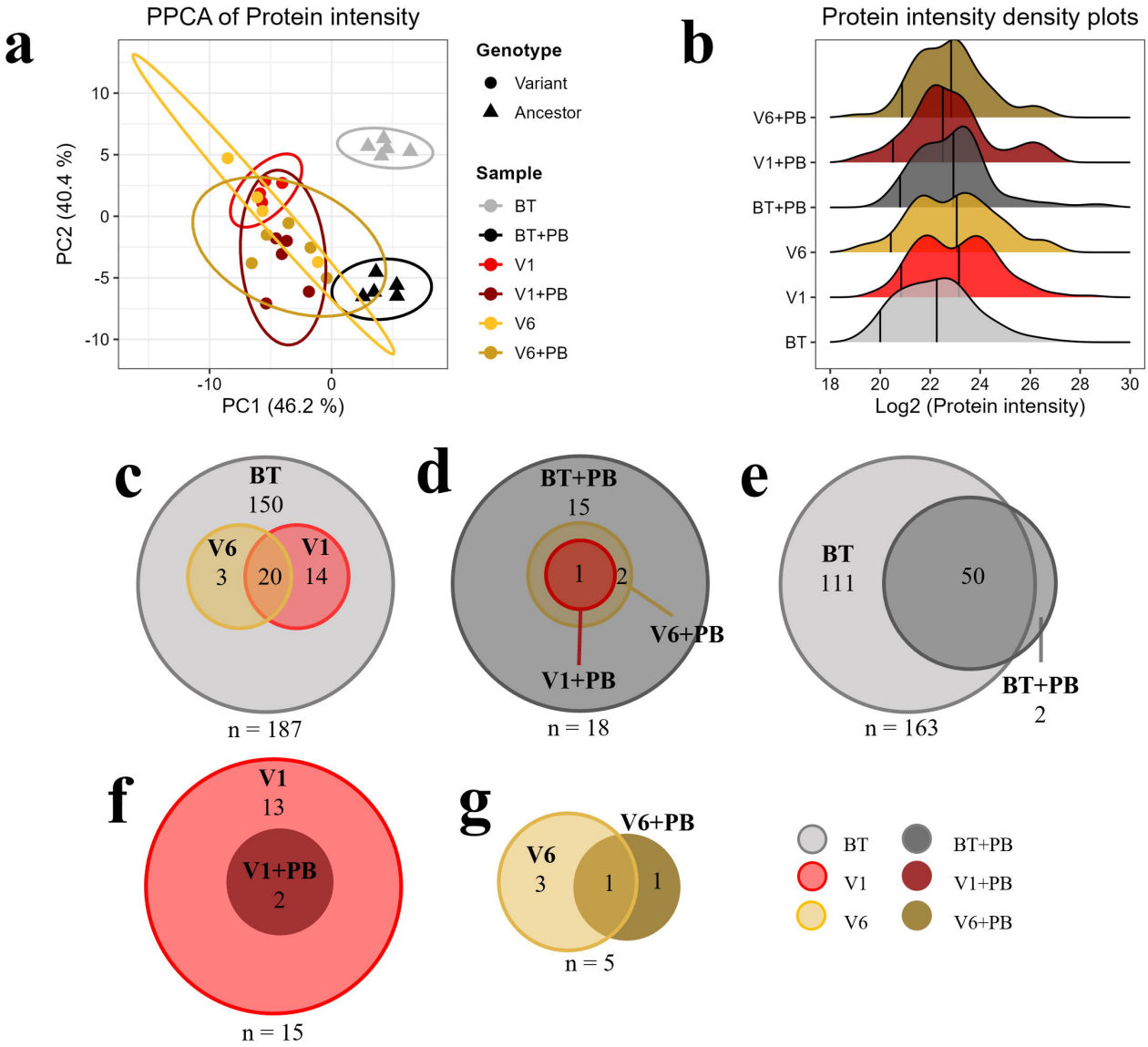
a
PPCA of Protein intensity
PC2 (40.4 %)
PC1 (46.2 %)
10
5
0
-5
-10
-10
0
Genotype
Variant
Ancestor
Sample
BT
BT+PB
V1
V1+PB
V6
V6+PB
b
Protein intensity density plots
V6+PB
V1+PB
BT+PB
V6
V1
BT
18
20
22
24
26
28
30
Log2 (Protein intensity)
c
BT
150
V6
3
20
V1
14
n = 187
d
BT+PB
15
1
2
V6+PB
V1+PB
n = 18
e
BT
111
50
BT+PB
2
n = 163
f
V1
13
V1+PB
2
n = 15
g
V6
3
1
V6+PB
1
n = 5
BT
V1
V6
BT+PB
V1+PB
V6+PB

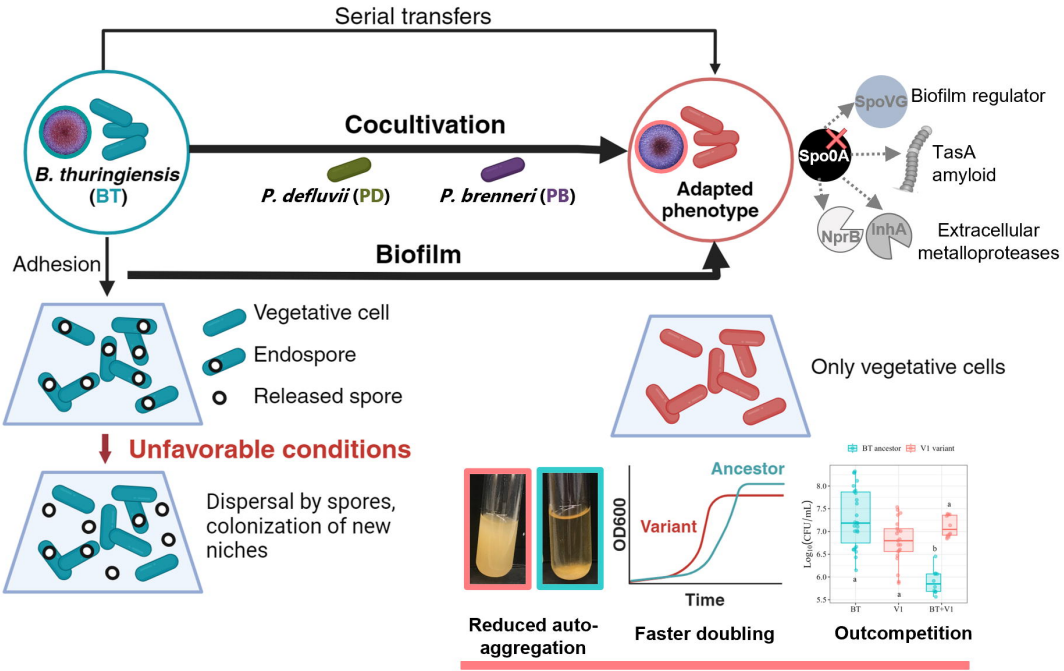
Serial transfers
B. thuringiensis (BT)
Cocultivation
P. defluvii (PD)
P. brenneri (PB)
Adapted phenotype
SpoVG
Biofilm regulator
Spo0A
TasA amyloid
NprB
InhA
Extracellular metalloproteases
Adhesion
Biofilm
Vegetative cell
Endospore
Released spore
Only vegetative cells
Unfavorable conditions
Dispersal by spores, colonization of new niches
Ancestor
Variant
OD600
Time
BT ancestor
V1 variant
Log10(CFU/mL)
BT
V1
BT+V1
Reduced auto-aggregation
Faster doubling
Outcompetition
Advantages over ancestor

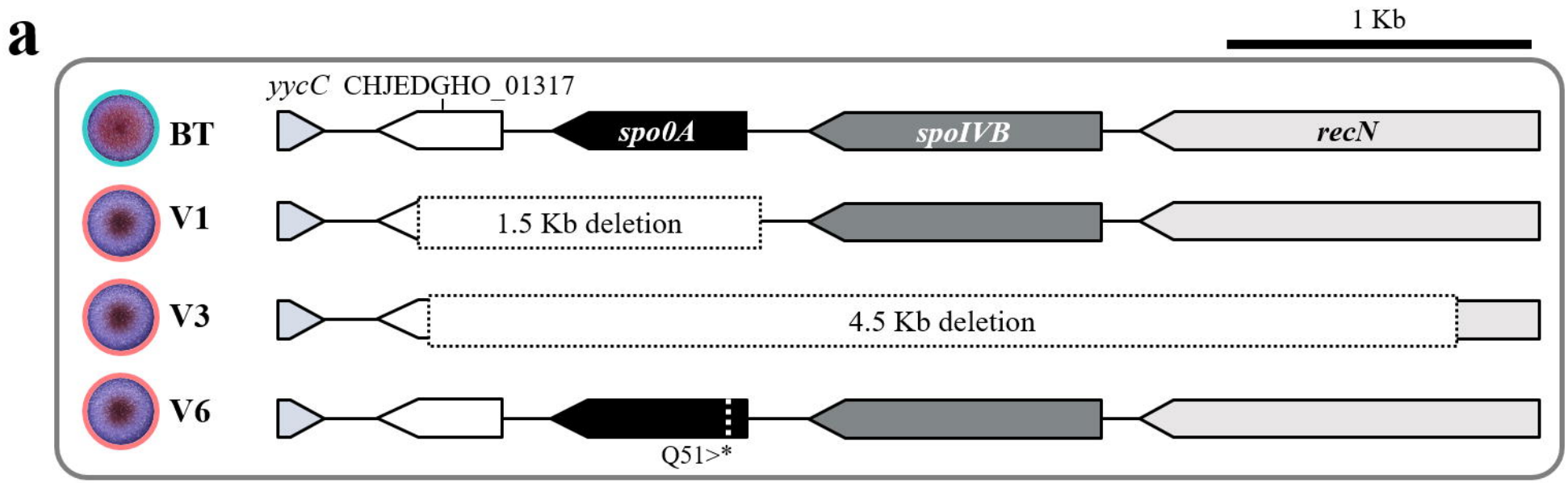
a
1 Kb
yycC CHJEDGHO_01317
BT
spo0A
spoIVB
recN
V1
1.5 Kb deletion
V3
4.5 Kb deletion
V6
Q51>*

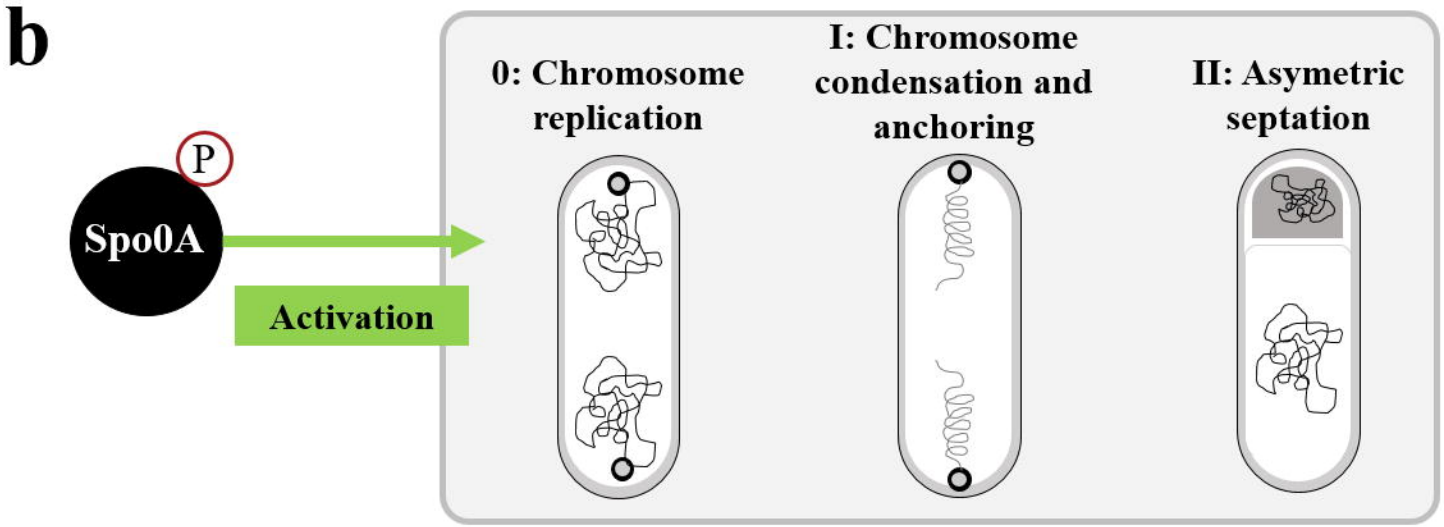
b
P
Spo0A
Activation
0: Chromosome replication
I: Chromosome condensation and anchoring
II: Asymetric septation

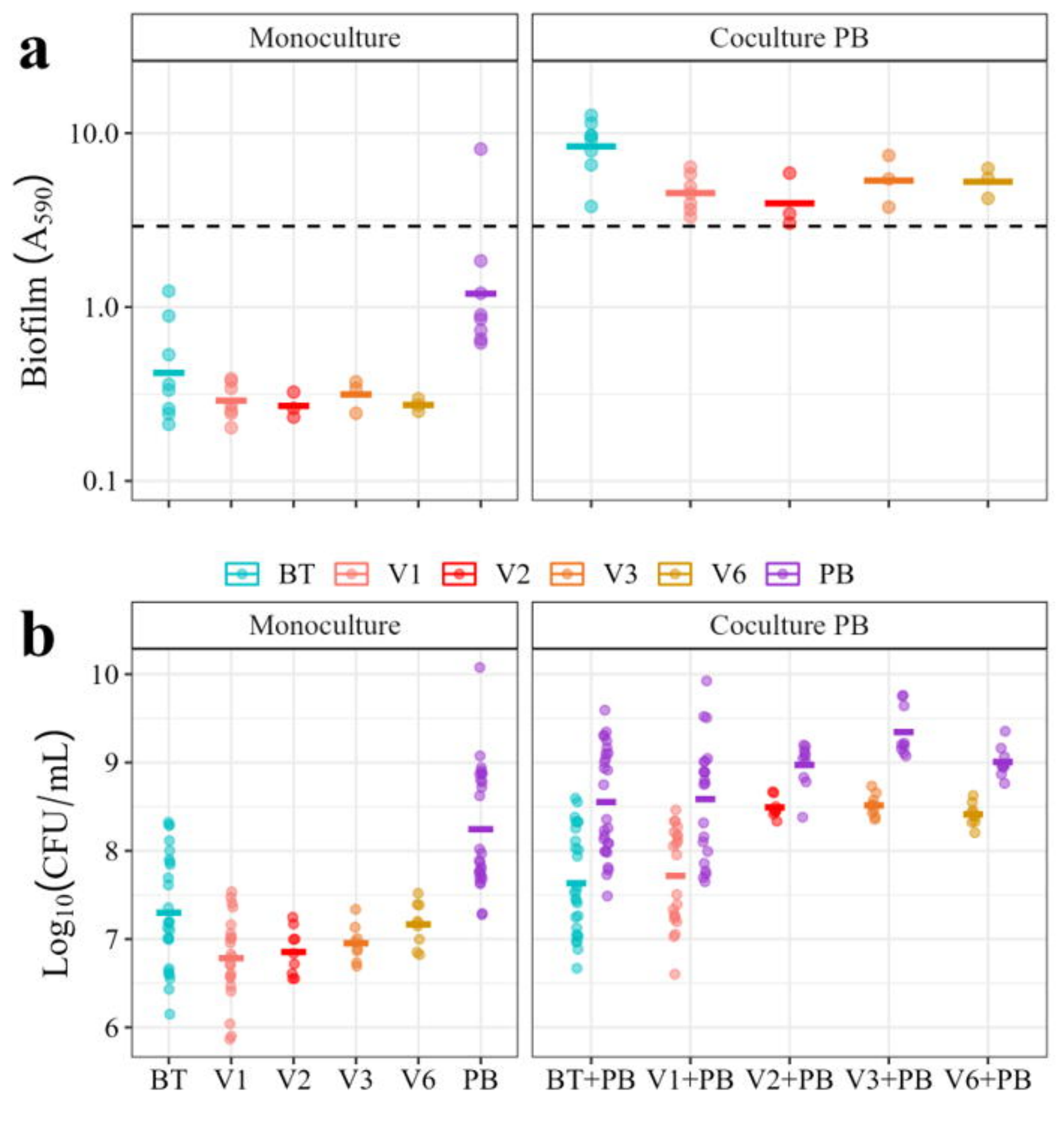
a
Monoculture
Coculture PB
Biofilm (A_{590})
10.0
1.0
0.1
BT
V1
V2
V3
V6
PB
b
Monoculture
Coculture PB
Log_{10}(CFU/mL)
10
9
8
7
6
BT
V1
V2
V3
V6
PB
BT+PB
V1+PB
V2+PB
V3+PB
V6+PB

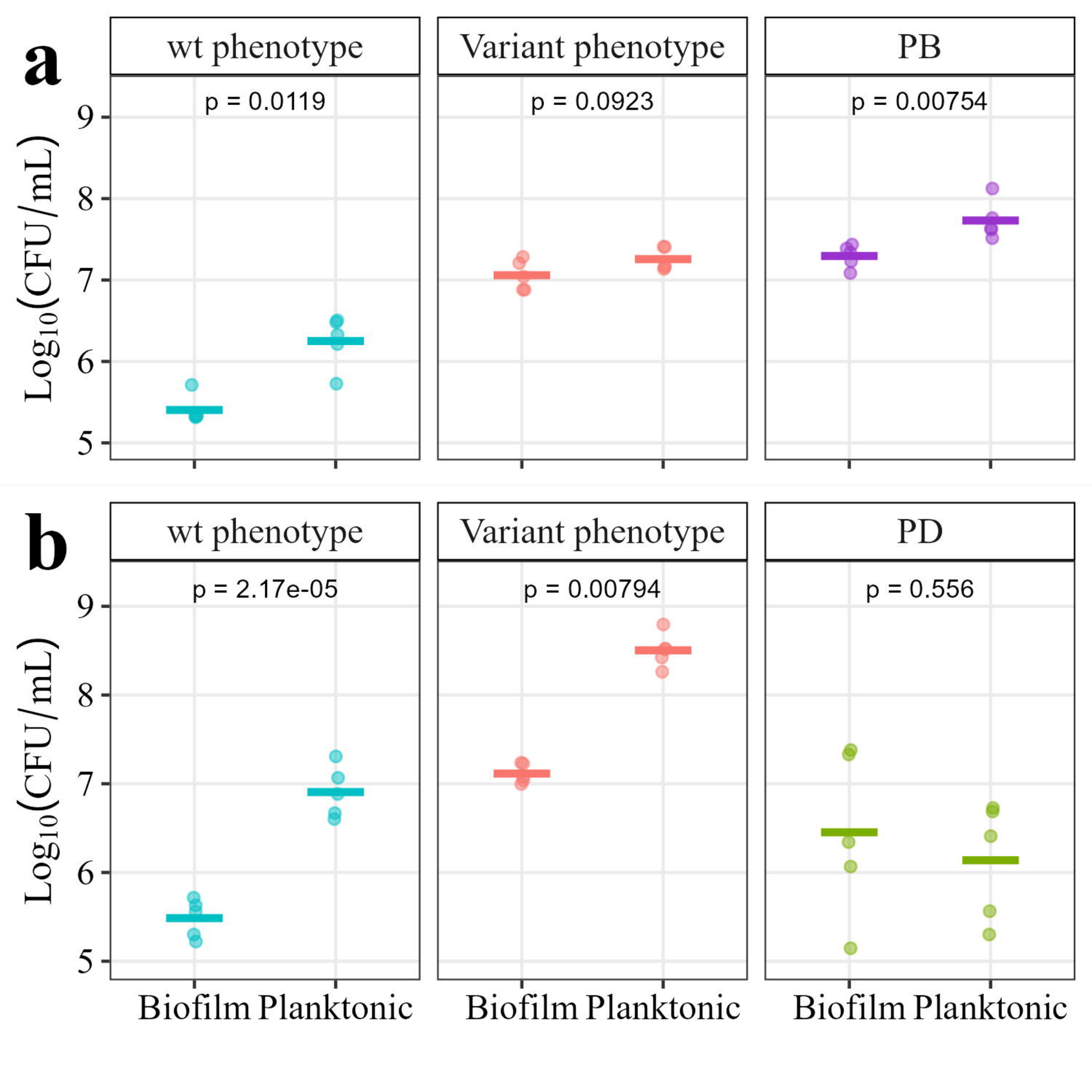
a
wt phenotype
Variant phenotype
PB
p = 0.0119
p = 0.0923
p = 0.00754
b
wt phenotype
Variant phenotype
PD
p = 2.17e-05
p = 0.00794
p = 0.556
Log10(CFU/mL)
9
8
7
6
5
Biofilm Planktonic
Biofilm Planktonic
Biofilm Planktonic

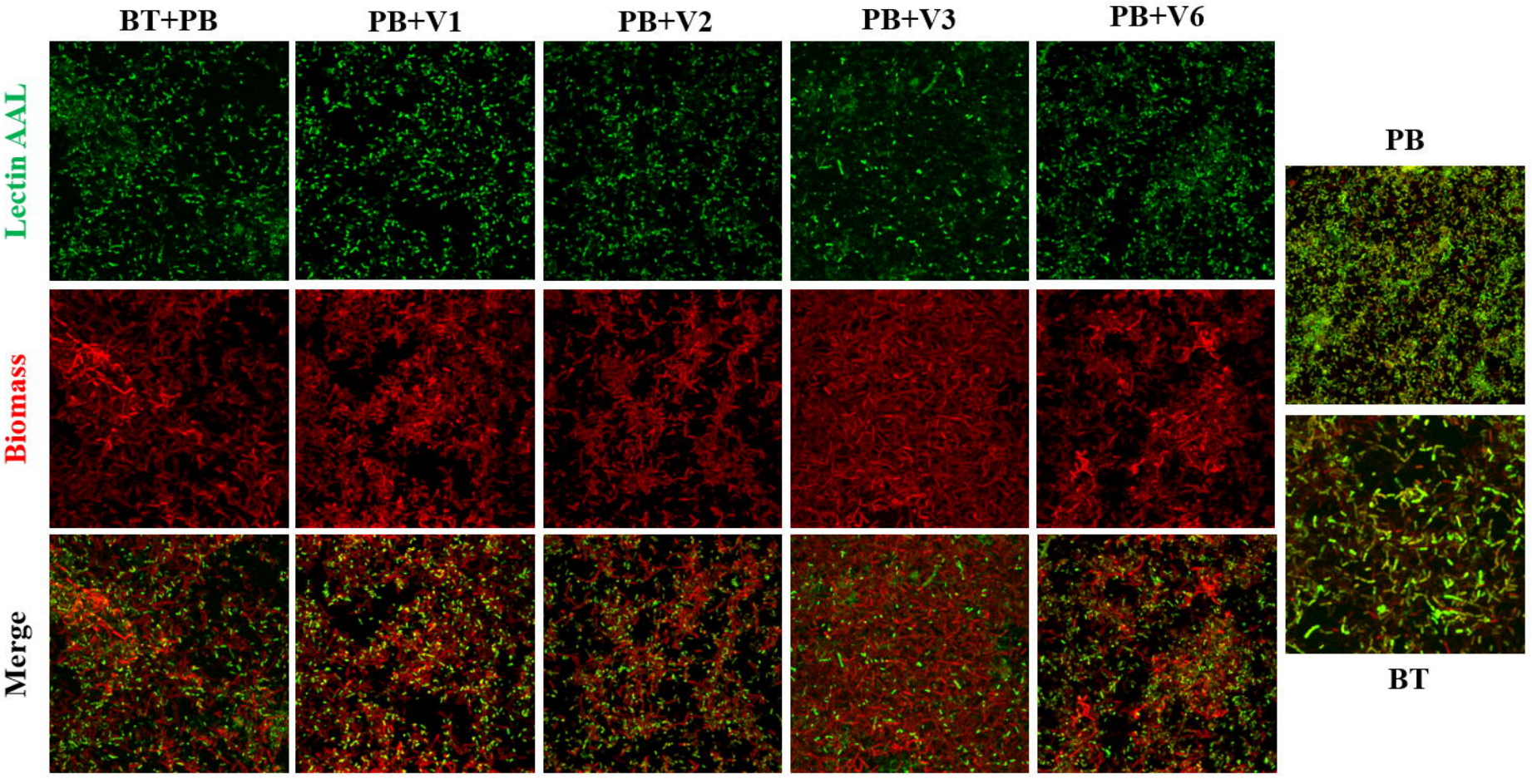
BT+PB
PB+V1
PB+V2
PB+V3
PB+V6
Lectin AAL
Biomass
Merge
PB
BT

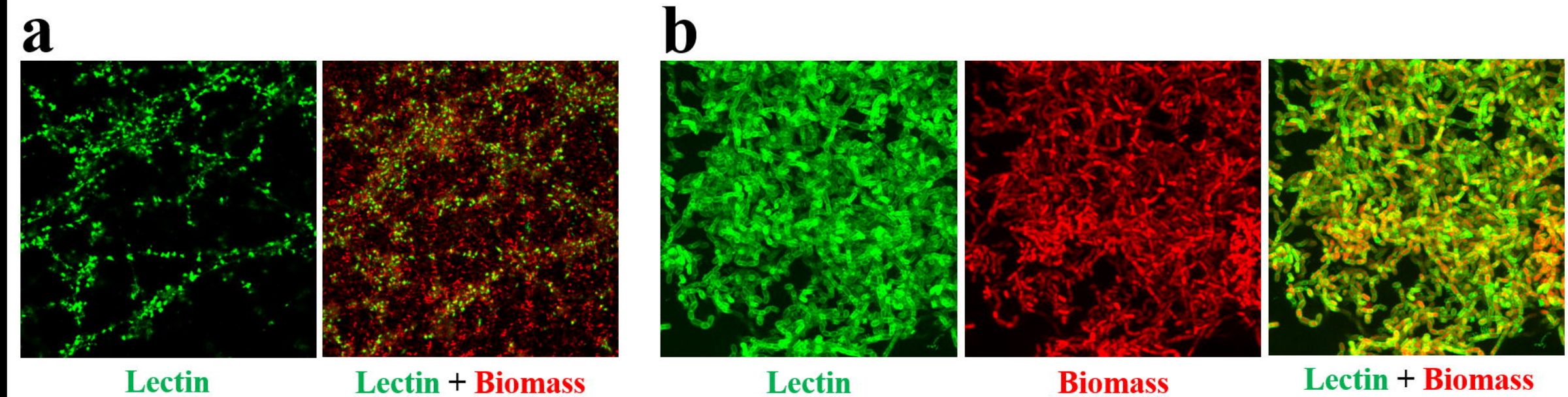
a
b
Lectin
Lectin + Biomass
Lectin
Biomass
Lectin + Biomass

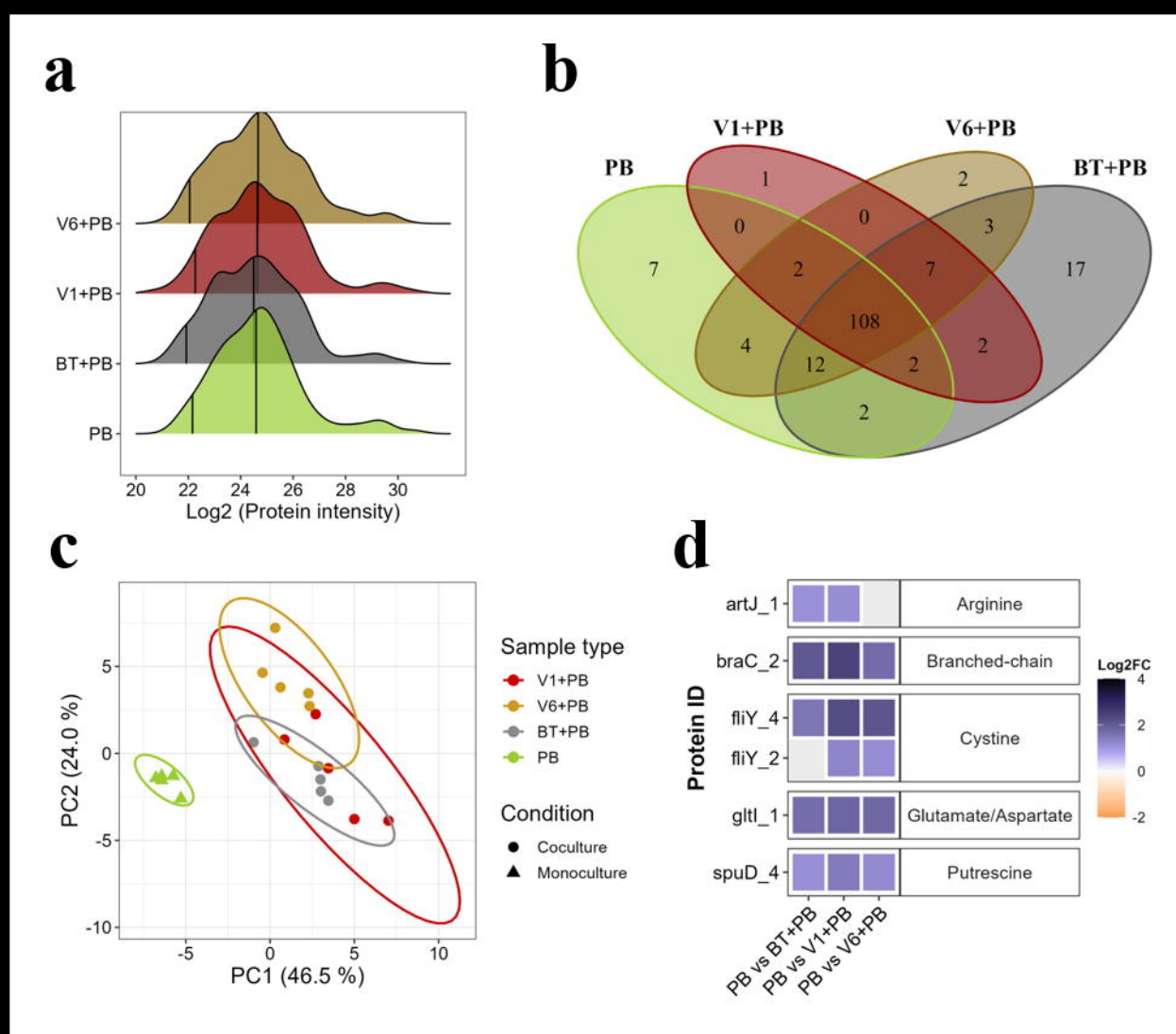
a
V6+PB
V1+PB
BT+PB
PB
20
22
24
26
28
30
Log2 (Protein intensity)
b
PB
V1+PB
V6+PB
BT+PB
1
2
0
0
3
7
2
7
17
108
4
2
12
2
2
c
PC2 (24.0 %)
PC1 (46.5 %)
5
0
-5
-10
-5
0
5
10
Sample type
V1+PB
V6+PB
BT+PB
PB
Condition
Coculture
Monoculture
d
Protein ID
artJ_1
braC_2
fliY_4
fliY_2
gltI_1
spuD_4
Arginine
Branched-chain
Cystine
Glutamate/Aspartate
Putrescine
Log2FC
4
2
0
-2
PB vs BT+PB
PB vs V1+PB
PB vs V6+PB

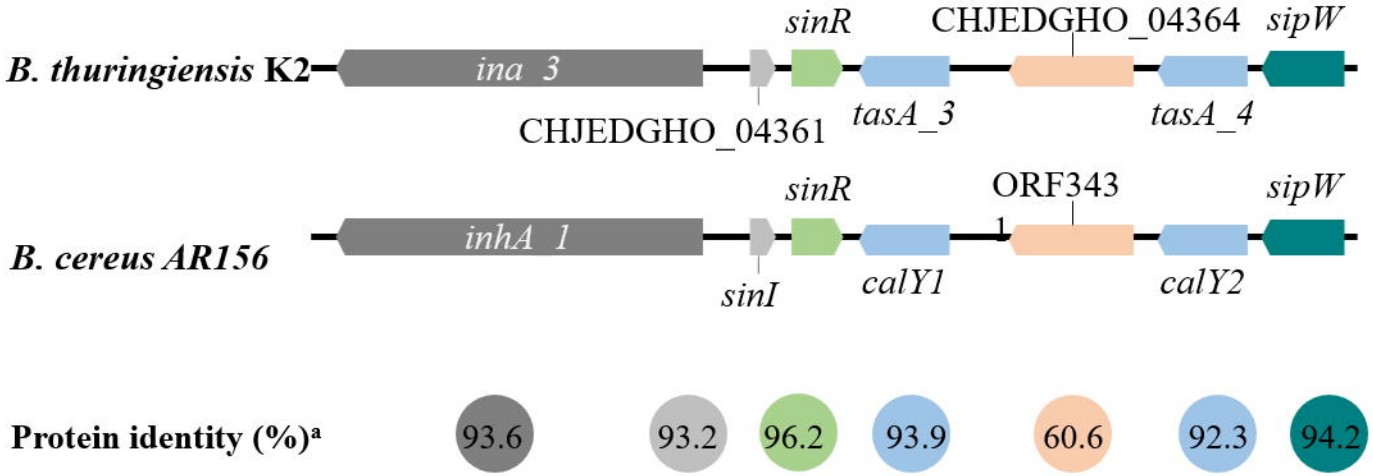
B. thuringiensis K2
ina_3
CHJEDGHO_04361
sinR
tasA_3
CHJEDGHO_04364
tasA_4
sipW
B. cereus AR156
inhA_1
sinI
sinR
calY1
ORF343
calY2
sipW
Protein identity (%)[a]
93.6
93.2
96.2
93.9
60.6
92.3
94.2